Available online at www.sciencedirect.com
ScienceDirect
International Journal of Heat and Mass Transfer 51 (2008) 2711–2732
International Journal of HEAT and MASS TRANSFER
www.elsevier.com/locate/ijhmt

Modeling the 3-D radiation of anisotropically scattering media by two different numerical methods

D.N. Trivic *, C.H. Amon [1]

Institute for Complex Engineered Systems, College of Engineering, Carnegie Mellon University, Pittsburgh, PA 15213, USA

Received 3 April 2007
Available online 20 December 2007

Abstract

An original model and code for 3-D radiation of anisotropically scattering gray media is developed where radiative transfer equation (RTE) is solved by finite volume method (FVM) and scattering phase function (SPF) is defined by Mie Equations (ME). To the authors' best knowledge this methodology was not developed before. Missing the benchmark, another new 3-D model and code, which solve the same problems, based on a combination of zone method (ZM) and Monte Carlo method (MC), as a solution of RTE, is developed. Here SPF is also calculated by Mie Equations. The conception ZM + MC is numerically expensive and is used and recommended only as a benchmark. The 3-D rectangular enclosure and the spherical geometry of particles are considered. The both models are applied: (i) to an isotropic and to four anisotropic scattering cases previously used in literature for 2-D cases and (ii) to solid particles of several various coals and of a fly ash. The agreement between the predictions obtained by these two different numerical methods for coals and ash is very good. The effects of scattering albedo and of wall reflectivity on the radiative heat flux are presented. It was found that the developed 3-D model, where FVM was coupled with ME, is reliable and accurate. The methodology is also suitable for extension towards: (i) mixture of non-gray gases with particles and (ii) incorporation in computational fluid dynamics.

Keywords: 3-D radiation; Anisotropically scattering; Finite volume method; Mie theory; Monte Carlo method; Zone method

1. Introduction

Radiation transfer within particulate media is important phenomenon in many scientific fields, processes and equipment. Some of these fields and equipment are: (i) combustion chambers where pulverized coal, char, soot or flay ash take place, (ii) cement kilns, (iii) fluidized beds, (iv) rockets with solid propellants, (v) pulsed lasers, (vi) remote sensing, (vii) optical tomography and (viii) energy emission from a nuclear explosion. The particles cloud emits, absorbs and scatters radiation energy where scattering is mainly anisotropic. There is a great interest nowadays in mathematical modeling of these phenomena as well as in their implementation. The developed models and codes are needed to be applied for the solution of various problems in engineering and science related to particles radiation.

There have been many publications considering the radiative heat transfer within multi-dimensional particulate media. Ratzel and Howell [1] used the P-3 spherical harmonic method for radiative transfer in absorbing, emitting and scattering media in 2-D rectangular enclosure. They presented their results for isotropic scattering. Fiveland [2] considered two-dimensional radiation using S-N discrete ordinate method (DOM) to solve radiative transfer equation. But he analyzed only the problems with isotropic scattering. Crosbie and Schrenker [3] solved the integral equation for radiative transfer in a two-dimensional rectangular enclosure by removing the singularity. They reported the predictions for isotropically scattering media. Menguc and Viscanta [4] analyzed radiative transfer in a 3-D

* Corresponding author. Present address: Brace Jovanovica 16-A, 26000 Pancevo, Serbia. Tel.: +381 13 344889.
E-mail address: trivic@bisinter.net (D.N. Trivic).
[1] Faculty of Applied Science and Engineering, University of Toronto, Toronto, Ontario M5S 1A4, Canada.

0017-9310/$ - see front matter © 2007 Elsevier Ltd. All rights reserved.
doi:10.1016/j.ijheatmasstransfer.2007.10.015

Nomenclature

a	coefficients of discretization equations
A	area of control volume faces
b	source term in discretization equations
$D^l_{cx}, D^l_{cy}, D^l_{cz}$	direction cosines integrated over solid angle control volume $\Delta\Omega$
E	emissive power
$\hat{e}_x, \hat{e}_y, \hat{e}_z$	unit vectors in x, y, and z directions
f_{ij}	total view factor or total interchange factor (TIF)
G	average incident radiation
$\overline{G_k G_i}$	total interchange area between volume zones k and i
$\overline{G_k S_i}$	total interchange area between volume zone k and surface zone i
i	$\sqrt{-1}$
i_1	non-dimensional polarized intensity
i_2	non-dimensional polarized intensity
I	intensity
I_B	blackbody intensity from an opaque wall
I_b	blackbody intensity from a medium
I_w	intensity at opaque diffuse wall
k	absorptive index (imaginary part of the complex index of refraction)
K	absorption coefficient
L	number of sub-control angles
L	maximal distance of travel
L	cube side
m	complex index of refraction
$\hat{n}$	unit outward normal vector
n	refractive index (real part of the complex index of refraction)
n	index in infinite series
q	heat flux
q_w	wall heat flux
Q_{sca}	scattering efficiency factor
Q^*_{ys}	non-dimensional net radiative heat flux in y-direction at the middle of south wall
Q^*_{zr}	non-dimensional net radiative heat flux in z-direction at the middle of rear wall
Q^*_{zf}	non-dimensional net radiative heat flux in z-direction at the middle of front wall
Q^*_z	non-dimensional net radiative heat flux in z-direction along the centerline
r	particle radius
$\vec{r}$	position vector
R_i	random number
$R(\xi)$	cumulative distribution function
s	distance traveled by a beam
$\hat{s}$	angular direction
S	source function
$\overline{S_j G_i}$	total interchange area between surface zones j and volume zone i
$\overline{S_j S_i}$	total interchange area between surface zones j and i
V	zone volume
x, y, z	Cartesian coordinate directions
x	particle size parameter
X, Y, Z	non-dimensional coordinates, $X = x/L$, $Y = y/L$, $Z = z/L$

Greek symbols

α	scattering angle, notation in Monte Carlo Method, same as γ and ψ
β	extinction coefficient, the angle between plane of incident beam and plane of scattered beam
γ	scattering angle designated within Mie theory, same as ψ
η	polar angle in Monte Carlo Method
$\Delta x, \Delta y, \Delta z$	control volume dimensions in x, y and z directions, dimensions of the zones in Monte Carlo method
ΔV	volume of control volume
$\Delta\Omega$	solid angle control angle
ε	wall emissivity
κ	absorption coefficient
κ_p	absorption coefficient of particles cloud
λ	the wavelength of incident radiation
μ	direction cosine in the x-direction, $\cos\theta$
ρ	wall reflectivity
θ	polar angle measured from $\hat{e}_z$ in FVM
θ	planar angle in Monte Carlo Method
σ	scattering coefficient or Stefan Boltzmann constant
τ_x, τ_y, τ_z	optical coordinates, βx, βy and βz respectively
$\tau_{xL}, \tau_{yL}, \tau_{zL}$	overall optical thicknesses, equal to βL
ϕ	azimuthal (planar) angle measured from $\hat{e}_x$
Φ	scattering phase function
$\Phi(\gamma)$	scattering phase function for γ argument
$\overline{\Phi}^{l'l}$	normalized scattering phase function, or average scattering phase function, or average energy scattered from solid control angle defined by direction l' to solid control angle defined by direction l
ξ	appropriate variables calculated from cumulative distribution function
ψ	scattering angle, same as γ

Superscript

*	non-dimensional variables
+	positive direction
−	negative direction
′	incident direction
l, l'	angular directions

Subscripts

b	blackbody
e, w, n, s, r, f	east, west, north, south, rear and front neighbors of control volume P
P	control volume P
p	related to particles
x, y, z	coordinate directions
w	wall
S	sub-control angle

Abbreviations

ADF	absorption distribution function
BC	boundary condition
CFD	computational fluid dynamics
DOM	discrete ordinate method
FV	finite volume, same as FVM
FVM	finite volume method
LBL	line-by-line (model)
MC	Monte Carlo, same as MCM
MCM	Monte Carlo method
ME	Mie Equations, same as MT
MT	Mie theory, same as ME
MOL	method of lines
ODE	ordinary differential equation
PDE	partial differential equation
PDF	probability density function
RTE	radiative transfer equation
SLW	spectral line-based weighted sum of gray gases (model)
SNB	statistical narrow band (model)
SPF	scattering phase function
TIA	total interchange area
TIF	total interchange factor
2-D	two dimensional
3-D	three dimensional
WSGGM	weighted sum of gray gases model
ZM	zone method

rectangular geometry using the first- and three-order spherical harmonics approximations. They presented the results for particulate media with anisotropic scattering by taking gray delta-Eddigton approximation as scattering phase function. Thynell and Ozisik [5] studied radiation transfer in rectangular geometries by using finite element method and their results are for isotropic scattering. From these five multi-dimensional cases cited above, four cases are for isotropic scattering and only one [4] for anisotropic scattering which, as the scattering phase function, has an approximation valid only for the particular particle parameter. Kim and Lee [6] modeled the radiative heat transfer in 2-D rectangular enclosures by using S-N discrete ordinate method to solve radiative transfer equation. The gray media in considered geometries absorb, emit and anisotropically scatter radiant energy. The scattering phase function was defined by Legendre polynomials expansions. Here the radiative intensity field, average incident radiation and the radiative heat flux were predicted. In addition the effects of: anisotropy of the scattering phase functions, the aspect ratio, the optical thickness, the scattering albedo and the boundary reflectivity on the radiative transfer were thoroughly examined. The two-dimensional anisotropic scattering cases evaluated there were presented then without comparison since there were no published results for those cases in that time.

A three-dimensional mathematical model for predicting turbulent flow with combustion and radiative heat transfer within a furnace has been developed by Trivic [7]. The model consists of two sections: (1) transport equations that are nonlinear partial differential equations solved by a finite difference scheme, and (2) the radiative heat transfer that was analyzed by the zone method. The Monte Carlo method was used to evaluate total radiative interchange in the system between zones. For the determination of the radiative properties of particles suspended in the combustion gases, the Mie equations were used. The mathematical model was validated against experimental data collected on two large furnaces: (1) A tangentially pulverized coal fired boiler of 220 MW; (2) an oil fired boiler of 345 MW, with symmetrically positioned burners at the front and rear wall. The results gave reasonable agreement between measurements and values predicted by the model.

A study related to the radiation of the mixtures of non-gray gas and particles in a pulverized-coal-fired boiler was done by Steward and Trivic [8]. The mathematical model based on the fundamental equations of motions and energy transfer, and on the zone method for determining radiative heat transfer, was developed for an operating 220 MW pulverized-coal-fired boiler. The scattering phase function, used for anisotropically scattering, was evaluated by Mie theory. The model is capable of predicting velocity, temperature and heat flux distributions for the three-dimensional combustion chamber. The calculated heat fluxes at the wall have been compared with experimental measurements taken on the boiler for three sets of operating conditions, and they indicated that confidence can be placed in the results.

In these models and codes [7,8] the Hottel and Cohen's zone method of analysis for energy balance coupled with the Monte Carlo method for the evaluation of total interchange factors (TIF) was a kind of solution of radiative transfer equation in that time.

The comparisons and evaluations of the predictions obtained by those conceptions [7,8] against the predictions of others related to particles radiation with anisotropically scattering, are difficult because the codes [7,8] did not deal with particles radiation only. Those 3-D codes link fluid flow, turbulence model, combustion pattern, heat transfer by convection, conduction and radiation, anisotropic

particles scattering and gas radiative properties models. Thus it was very difficult here to carry out the analysis of the role played only by the particles radiation with anisotropically scattering.

Yu et al. [9] presented an extension of WSGGM to a mixture of non-gray gas and gray particles. They used discrete ordinates method for the solution of radiative transfer equation which was coupled with WSGGM. In that paper the relation between the weighting factors used in the WSGGM for a mixture of non-gray gas and gray particles with scattering, when the thermal non-equilibrium exist, i.e. the gas and particles temperature are different, has been discussed. This model was applied to two cases. First case was a one-dimensional isothermal mixture of non-gray gas (CO_2, H_2O and transparent inert gas) and soot particles. They used the Smith et al. WSGGM gas radiative properties model [10] for the mixture of CO_2, H_2O and a transparent inert gas. The algebraic expression based on Rayleigh small particles limit [11], was used for the evaluation of soot absorption coefficient. Second calculation case consisted of a pure scattering medium in a cylindrically symmetric geometry and was used to examine the effect of anisotropy on radiative heat flux. The scattering phase function was presented by the approximation of a finite series of Legendre polynomials.

Solovjev and Webb [12] presented an efficient method for modeling radiative transfer in multi-component gas mixture with soot. The method is based on the spectral line weighted sum of gray gases (SLW) model. The gas mixture was considered as a single gas whose absorption distribution function (ADF) was evaluated through the distribution functions of the individual components in the mixture. The soot was taken as another gas in the mixture. The verification of the method was carried out by the comparison with line-by-line (LBL) solution for radiative transfer equation for mixtures of water vapor, carbon dioxide and carbon monoxide with various volume fractions of soot. Their predictions were compared against the previously published results calculated by statistical narrow band (SNB) model and by WSGGM [13]. The predictions were done for one-dimensional geometry and related to particles material only for soot particles. The calculation of soot absorption coefficient was done by using the Rayleigh small particles limit [11]. In that expression the absorption coefficient is an algebraic relation that depends on real and imaginary part of the complex index of refraction, soot volume fraction and medium temperature.

Ayranci and Selcuk [13] developed a methodology based on method of lines solution of discrete ordinates method for solution of the 3-D transient radiative transfer equation. Method of lines (MOL) consists of converting the system of partial differential equations (PDF) into an ordinary differential equation (ODE) initial value problem. It is done by discretizing the spatial derivatives and integrating the resulting ordinary differential equations by a sophisticated ODE solver. The method was applied for the prediction of transient and steady state transmittances in a cubical geometry. The considered medium in the enclosure is purely isotropically scattering i.e. having both, scattering coefficient and scattering phase function equal to unity. The predictions were validated against the Monte Carlo solutions found in the literature. It appeared that the method is flexible for implementation of linear spatial differencing scheme, flux limiters and weighted essentially non-oscillatory methods. In addition, it was found that Van Leer flux limiter provides stable, accurate and efficient solution.

Coelho [14] demonstrated a new method based on a hybrid finite volume/finite element discretization of the radiative transfer equation. The method was applied to multi-dimensional rectangular enclosures with gray absorbing–emitting–scattering media. In this approach the spatial discretization was performed by using finite volume method and angular discretization by basis functions commonly employed in the finite volume method. The comparisons of the predictions for two- and three-dimensional enclosures against the results calculated by analytical solution showed that the numerical solution converges to the analytical one as the discretization is refined. In this study the gray delta-Eddigton approximation as scattering phase function was used. This approximation is defined for a specific type of particulate medium.

Trivic et al. [15] developed a new mathematical model and code for radiative heat transfer of particulate media with anisotropic scattering for 2-D rectangular enclosure. The model is based on the coupling of (i) finite volume method for the solution of radiative transfer equation with (ii) Mie equations for the evaluation of scattering phase function. The predictions were compared against the only found results, published 15 years ago [6]. For those results [6] the S-N discrete ordinates method for the solution of radiative transfer equation and the Legendre polynomials expansions for the evaluation of scattering phase function were used. The agreement between the results in [6,15] is very good. The advantages of new model and code [15] are in their straight forward application to any given particles parameters without the need for previously designed analytical expression for scattering phase function. In addition, that analytical expression, with generated expansion coefficients, is restricted and can be used only for that particular case of particle parameters. The new model was applied to the solid particles of several various coals and of an ash and the series of 2-D predictions are performed. The effects of particle size parameter and of scattering albedo on radiative heat flux and on incident radiation were analyzed. It was found that the model developed is reliable and very accurate and thus suitable for extension towards (i) 3-D geometries, (ii) mixtures of non-gray gases with particles as well as for (iii) incorporation in computational fluid dynamics codes.

Many previous works which consider particles radiation are incomplete and have the drawbacks from the point of view of generality, engineering modeling and industrial applications. They usually deal with: (i) isotropic scatter-

ing, (ii) 1-D or 2-D geometries, (iii) scattering phase function (SPF) as an approximation, i.e. as Legendre polynomials expansions, delta-Eddigton approximation etc., valid only for that particular particle's parameters and (iv) an arbitrary value of scattering coefficient which is not related to any particle's parameters.

The radiation under the real conditions is mainly tridimensional. Considering the gray delta-Eddigton phase function approximation, used in [4,14], it should be noticed that this function is not general. It mainly accounts for highly forward scattering of the particles. All these approximations of SPF as Legendre polynomials expansions [6,9], delta-Eddigton approximation [4,14] etc., can be used only for very specific cases.

What is missing in literature, but always needed in engineering modeling and in industrial application is a 3-D more general model and code for the radiation of particulate media with non-isotropic scattering. Here the scattering phase functions should not be arbitrarily taken but have to be related to the parameters of real particles, i.e to the particles existing in that enclosure. These parameters of particle are particles diameter, complex refractive index, wavelength of incident radiation etc.

The 2-D analysis [15] was performed for the sake of comparison against only available benchmark [6] and for the sake of validation of the methodology, because for 3-D particles radiation with anisotropic scattering hardly can be found any benchmark case. The two-dimensional version of the code [15] has been successfully tested against the predictions reported in Ref. [6] for isotropic and anisotropic scattering. The advantages and the benefits of the 2-D model presented in Ref. [15], compared with other conceptions, is discussed and proved in [15], and it will not be repeated here. The simile merits can be expected for the methodology extension to 3-D cases.

In the present study two tasks have been done. First is the extension of the methodology developed in [15], based on the coupling of Finite Volume Method with Mie Equations, to three-dimensional geometries. It was never done before to the best knowledge of authors. Second is, because of the lack of the benchmark for the validation of these 3-D predictions, the development of a new model and code for generating the benchmark results.

Thus the predictions calculated by 3-D FVM with ME had to be compared against the results calculated by another original model and code which should use complete different numerical techniques. The new model and code developed here for benchmark are based on a combination of 3-D Zone Method (ZM) with Monte Carlo Method (MCM). Because this conception (ZM + MCM) is numerically expensive, i.e. time consuming and inconvenient for engineering modeling, it was used and is suggested only as a benchmark.

It is believed that this model, 3-D FVM with ME, is reliable, accurate and convenient for engineering applications. Also, once this methodology is validated, it can be used for more complex modeling as 3-D radiation of mixtures of non-gray gases with gray and with non-gray particles, as well as to be incorporated in CFD codes.

2. Mathematical formulations

2.1. Governing equations for finite volume method coupled with Mie theory

2.1.1. Radiative transfer equation for 3-D particulate media

The particulate medium in this study is considered as a gray medium. The equation for 3-D radiative heat transfer for a gray medium is given in more references by various authors, as by Ozisik [15], Siegel and Howell [16] and Modest [17]. It is given as

$$\frac{\mathrm{d}I(\vec{r},\hat{s})}{\mathrm{d}s} = -\beta(\vec{r})I(\vec{r},\hat{s}) + S(\vec{r},\hat{s}) \tag{1}$$

This equation means that the change of intensity along a path, or the energy accumulation, is equal to the difference between the energy gained and energy lost. The term $-\beta(\vec{r})I(\vec{r},\hat{s})$ presents attenuation and term $S(\vec{r},\hat{s})$ accounts for augmentation.

The extinction coefficient β, is given as

$$\beta(\vec{r}) = \kappa(\vec{r}) + \sigma(\vec{r}) \tag{2}$$

where $\kappa(\vec{r})$ represents the absorption of radiant energy and $\sigma(\vec{r})$ accounts for the out-scattering of radiant energy.

The energy source function, $S(\vec{r},\hat{s})$, is calculated as

$$S(\vec{r},\hat{s}) = \kappa(\vec{r})I_b(\vec{r}) + \frac{\sigma(\vec{r})}{4\pi}\int_{4\pi} I(\vec{r},\hat{s}')\Phi(\hat{s}',\hat{s})\,\mathrm{d}\Omega' \tag{3}$$

The first term of the right hand side of this expression, $\kappa(\vec{r})I_b(\vec{r})$, accounts for gas emission while the second term represents the accumulation of radiant energy due to in-scattering from all other directions in the domain.

Radiant intensity I depends on spatial position $\vec{r}$ and angular direction $\hat{s}$. For 3-D rectangular enclosure, I depends on five spatial variables, $I(x, y, z, \theta, \phi)$. Here x, y, z are the Cartesian coordinates of the position vector, $\vec{r}$, and θ, ϕ are the polar and planar angles respectively that define the intensity direction $\hat{s}(\theta,\phi)$.

The scattering phase function, $\Phi(\hat{s}\prime,\hat{s})$, is equal to unity for isotropic scattering and has various values in various directions, $(\hat{s}',\hat{s})$, for anisotropic scattering.

2.1.2. Discretized form of 3-D radiative transfer equation

Detailed procedure of discretization of 3-D radiative transfer equation and of source function for finite volume method is presented in several sources as [18–20]. Therefore this will not be derived and discussed here again. Only final discretized equations needed for the explanation of the link with Mie theory will be considered and used herewith. Also the radiative heat transfer relations as the incident radiation coming from all directions (i.e., integrated over 4π radians), $G(\vec{r})$, the radiative heat flux in the direction of the unit vector $\hat{i}$ expressed as $q_i(\vec{r})$ and the divergence of

the radiative heat flux, designated by $\nabla \bullet q$, used in this work, are presented in details in sources [18,20,21] and it will not be discussed here once again.

By integrating Eq. (1) over control angle and control volume and after that by applying the divergence theorem on its left hand side, Eq. (1) is transformed towards discretization. In finite volume method, the magnitude of the radiative intensity is taken constant over the control angle and control volume. Under these assumptions, for six control volume faces, i.e. for 3-D geometry, Eq. (1) can be written in a simple way as

$$\sum_{i=1}^{6} I_i^l A_i \int_{\Delta\Omega_l} (\hat{s}^l \bullet \hat{n}_i)\mathrm{d}\Omega = \int_{\Delta\Omega^l} \int_{\Delta V} (-\beta I^l + S^l)\mathrm{d}V\,\mathrm{d}\Omega \quad (4)$$

where source function written in discretization form is

$$S^l = \kappa I_b + \frac{\sigma}{4\pi} \sum_{l'=1}^{L} I^{l'} \overline{\Phi}^{l'l} \Delta\Omega^{l'} \quad (5)$$

In Eq. (5), the quantity $\overline{\Phi}^{l'l}$ is the average scattering phase function from control angle l' (that is incident angle) to control angle l (that is scattering angle). This average scattering phase function is the link with Mie theory, i.e. it will be evaluated by using Mie equations.

The areas, or six control volume faces, A_e, A_w, A_n, A_s, A_f and A_r are defined as

$$A_e = A_w = \Delta y \Delta z, \quad A_n = A_s = \Delta x \Delta z, \quad A_f = A_r = \Delta x \Delta y \quad (6)$$

The volume of control volume is denoted as

$$\Delta V_P = \Delta x \Delta y \Delta z \quad (7)$$

The areas A_e and A_w are equal for Cartesian coordinates, but the different symbols are used for the sake of generality. The same is for areas A_n and A_s as well as for areas A_f and A_r.

To relate the intensity at the boundaries of control volumes to the nodal intensities, spatial differencing schemes are needed. One of the available schemes is the step scheme, which sets the downstream boundary intensities equal to the upstream nodal intensities. The step scheme was used within this study.

A more compact form of discretization equation suitable for control volume pointing in all directions (and for various marching procedure following directions cosine) is written as

$$a_P^l I_P^l = a_W^l I_W^l + a_E^l I_E^l + a_S^l I_S^l + a_N^l I_N^l + a_R^l I_R^l + a_F^l I_F^l + b^l \quad (8)$$

where b_l is source term in discretization equation and is calculated as

$$b_l = S_P^l \Delta V_P \Delta\Omega^l \quad (9)$$

Eq. (8) is used to calculate the new values of radiant intensities, and they are calculated as follows:

$$I_P^l = \frac{a_W^l I_W^l + a_E^l I_E^l + a_S^l I_S^l + a_N^l I_N^l + a_R^l I_R^l + a_F^l I_F^l + b^l}{a_P^l} \quad (10)$$

Detailed derivation and presentation of the other variables related to the discretization is given in [18–20] and it will not be given here again.

2.1.3. Discretized boundary conditions

For an opaque diffuse surface, the boundary condition given in the form of the boundary intensity is

$$I(\vec{r},\hat{s}) = \varepsilon(\vec{r}) I_b(\vec{r}) + \frac{\rho(\vec{r})}{\pi} \int_{\hat{s}' \bullet n<0} I(\vec{r},\hat{s}')|\hat{s}' \bullet \vec{n}|\,\mathrm{d}\Omega' \quad (11)$$

On the right hand side of Eq. (11) there are two expressions. The first one is the emission due to the surface temperature where I_b is the so-called black body radiation. The second term is the reflection of the incoming intensities. The radiation energy leaving an opaque diffusion surface is just the sum of these two effects.

The discretized form of Eq. (11) is as follows:

$$I_w = \varepsilon_w I_B + \frac{\rho_w}{\pi} \sum_{D_{cx}^{l'}} I_w^{l'} D_{cx}^{l'} \quad (12)$$

This, so-called temperature boundary condition, was used for the problems analyzed in this study within the computer codes developed here. When the heat flux at the wall is prescribed, the intensity leaving that diffuse, opaque wall is given in discretized form as

$$I_w = \frac{q}{\pi} + \frac{1}{\pi} \sum_{D_{cx}^{l'}} I_w^{l'} D_{cx}^{l'} \quad (13)$$

The other types of boundary conditions as Symmetry Conditions, Periodic Conditions etc, and their detailed description as well as the explanation of the variables can be found in Chai's Ph.D. Thesis [18,20]. If it is needed, the discretized form of those boundary conditions can be easily incorporated in the code developed here.

2.1.4. The link of control volume method with Mie theory

The radiation incident on a solid particle is partly absorbed and partly scattered. The scattering is a dispersion of part of the incident radiant energy in different directions. The fraction of the energy that is scattered into any given direction, defined by scattering angle γ is given by Scattering Phase Function as

$$\Phi(\gamma) = 2\frac{i_1 + i_2}{x^2 Q_{\mathrm{sca}}} \quad (14)$$

The quantities i_2 and i_2 are the non-dimensional polarized intensities, x is particle size parameter and Q_{sca} is efficiency factor for scattering. The calculation of Scattering Phase Function (SPF), as well as the all relevant variables related to Eq. (14), are discussed and presented in details in Appendix A of the Ref. [26] and it will not be repeated here.

A rigorous theory of radiative infrared waves interacting with solid particles, developed for several simple geometries, i.e. for spherical and cylindrical particles, has been presented by Van de Hulst [22]. The mathematical description of the interaction between incident radiation and a sin-

gle solid particle is presented with Maxwell's wave equations. The solution to this problem was obtained by Gustav Mie [22,23], who solved Maxwell's wave equations with the appropriate boundary conditions for single cylindrical and spherical particles. The same problem was solved by Danish physicist Lorenz [24] without using the Maxwell's equations. Lorenz developed his own theory of electromagnetism. Although Lorenz's work predates that of Mie, the general theory related to the scattering of radiation by absorbing spheres is known as "Mie Theory".

Mie theory has been presented in many sources as by Van de Hulst [22], Hottel and Sarofim [25] and Modest [17]. The brief theoretical background and the basic equations and functions of Mie theory are summarized by Trivic et al. in Appendix A of the Ref. [26]. In that reference the application of Mie equations for 2-D anisotropic scattering coupled with Finite Volume Method is presented.

What is needed by Finite Volume Method related to anisotropic scattering is the average scattering phase function, $\overline{\Phi}^{l'l}$, to be used, i.e. substituted in Eq. (5). This average scattering phase function is also called in literature as the normalized scattering phase function. It gives average energy scattered from solid control angle defined by incident direction l' to solid control angle defined by direction l.

There are two different ways to evaluate the normalized scattering phase function $\overline{\Phi}^{l'l}$. They are: (1) the way when analytical expression for scattering phase function exists (various approximations as a finite series of Legendre polynomials etc.) and (2) the way when analytical expression for scattering phase function does not exist and scattering phase function will be evaluated through complex procedure related to Mie equations.

The first way when the analytical expression for scattering phase function exists, the average scattering phase function can be calculated then as

$$\overline{\Phi}^{l'l} = \frac{\int_{\mathrm{d}\Omega^{l'}} \Phi(\hat{s}', \hat{s})\,\mathrm{d}\Omega'}{\Delta\Omega^{l'}} \tag{15}$$

The second way, when the analytical expression for scattering phase function does not exist, the average scattering phase function is calculated as

$$\overline{\Phi}^{l'l} = \frac{\int_{\Delta\Omega^{l}} \int_{d\Omega^{l'}} \Phi(\hat{s}', \hat{s})\,\mathrm{d}\Omega'\,\mathrm{d}\Omega}{\Delta\Omega^{l}\Delta\Omega^{l'}} = \frac{\sum_{l_S=1}^{L_S} \sum_{l'_S=1}^{L'_S} \Phi^{l'_S l_S} \Delta\Omega^{l'_S} \Delta\Omega^{l_S}}{\Delta\Omega^{l}\Delta\Omega^{l'}} \tag{16}$$

The analytical expressions for the scattering phase functions for various particle materials considered within this study do not exist. Thus Eq. (16) is used in this work. The detailed derivation of Eq. (16) is presented and discussed in Ref. [20].

The calculation procedure is the following. The average scattering phase function, $\overline{\Phi}^{l'l}$ evaluated by Eq. (16) and used in Eq. (5) for calculation of source function, S^{l}, depends inter alia on the discrete values of scattering phase function, i.e. on $\Phi^{l'_S l_S}$ values. The values of $\Phi^{l'_S l_S}$ are in turn evaluated from Mie equations using Eq. (14).

That is the link of finite volume method with Mie theory.

The derivation and explanation of Eq. (14), which is used for calculation of the discrete values of scattering phase function, is presented in more details in Refs. [17,22,25,26].

It should be noticed here that $\Phi^{l'_S l_S}$ and $\Phi(\gamma)$ is the same expression having two different designations, where $\Phi(\gamma)$ comes from Mie theory notation and $\Phi^{l'_S l_S}$ is used within evaluation of average scattering phase function. Therefore the following expression can be written:

$$\Phi^{l'_S l_S} = \Phi(\gamma) = 2\frac{i_1 + i_2}{x^2 Q_{\mathrm{sca}}} \tag{17}$$

It should be noticed that in Eq. (16) each of the solid angle sub-control angle, i.e. $\Delta\Omega^{l'_S}$ and $\Delta\Omega^{l_S}$, for incident and scattering direction respectively, is defined with two, polar and asimuthal, angles and that the summation over each of them should be performed. Therefore, in Eq. (16), double summation sign in denominator will be transformed into four summation signs and those have been introduced in the code during the computer program editing.

The values of scattering angles which are defined by the sub-control angles $\Delta\Omega^{l'_S}$ and $\Delta\Omega^{l_S}$, i.e. for the incident and scattering directions $\widehat{S}'$ and $\widehat{S}$ respectively, must be known, i.e. previously defined, and then for them as the arguments, the values of scattering phase function can be evaluated. Those scattering angles are evaluated by applying the following expression:

$$\cos\psi = \mu\mu' + (1-\mu^2)^{1/2}(1-\mu'^2)^{1/2}\cos(\varphi' - \varphi) \tag{18}$$

Once the scattering angle ψ, designated as γ in Mie equations, is evaluated by Eq. (18), the scattering phase function $\Phi^{l'_S l_S}$ for that value of scattering angle, for given particles parameters as particle diameter D_p and complex index of refraction m and for known wavelength of incident radiation λ (or for given particle size parameter x) is calculated by using Eq. (17). Also it could be written that $\Phi^{l'_S l_S} = \Phi(\gamma, D_p, m, \lambda)$.

Therefore the value $\Phi^{l'_S l_S}$ that is the value of scattering phase function for the scattering from a discrete incident direction $\widehat{S}'$ into discrete scattering direction $\widehat{S}$ must be known before Eq. (16) can be applied.

Usually for the evaluation of average scattering phase function, the researchers as Kim and Lee [6] and Chai et al. [19] have used Eq. (15), i.e. they have used the analytical expression for scattering phase function that was the approximation by a finite series of Lagendre polynomials. Whenever a reliable analytical expression for scattering phase function exists, it is much simpler to apply Eq. (15) than Eq. (16). In this study, not having and using analytical expressions, the evaluation of average scattering phase function was carried out by applying Eq. (16) and by using Mie equations.

It should be mentioned that to the authors' best knowledge, among other things the implementation and validation of Eq. (16) for the radiation of anisotropically scattering media, except in only one case i.e. in Ref. [26], is never reported in literature so far.

2.2. Governing equations for zone method linked with Monte Carlo Method

2.2.1. Zone method for calculation of radiative heat transfer

One of the numerical techniques for solving radiative transfer equation which divides the system into a number of finite elements, known as the zone method of analysis, was developed by Hottel and Cohen [27]. It is also presented and explained in Ref. [25].

In the zone method the enclosure and its surrounding surfaces are divided into a number of volume and surface zones each of which is assumed to have uniform properties. A radiative energy balance is written on each zone giving the net radiative heat transfer between that zone and every other volume and surface zone in the system.

For a given surface zone i a radiative energy balance, considering the interaction between that surface zone i and all other surface zones j and volume zones k in the enclosure, can be written as

$$Q_{s,i(\mathrm{net})} = \sum_j \overline{S_jS_i} E_{s,j} + \sum_k \overline{G_kS_i} E_{g,k} - \varepsilon_i A_i E_{s,i} \tag{19}$$

Here $Q_{s,i(net)}$ is the net heat rate on the surface zone i and $\overline{S_jS_i}$ and $\overline{G_kS_i}$ are the total interchange areas. First expression on the right hand side of Eq. (19) gives the radiative energy received from all surface zones in the system, second term accounts for radiative energy received from all volume zones of the enclosure and third term is the radiative heat emitted by the surface zone i.

Similarly the radiative energy balance on a volume zone can be expressed as

$$Q_{g,i(\mathrm{net})} = \sum_j \overline{S_jG_i} E_{s,j} + \sum_k \overline{G_kG_i} E_{g,k} - 4K_iV_iE_{g,i} \tag{20}$$

where $Q_{g,i(\mathrm{net})}$ is the net heat rate in the volume zone$i$, also called volumetric radiative heat source, and $\overline{S_jG_i}$ and $\overline{G_kG_i}$ are the total interchange areas for radiative energy related to volume zone i.

There are two methods for calculating these total interchange areas: (1) the Determinant Method and (2) the Monte Carlo Method.

In this study the total interchange areas are defined by the Monte Carlo Method.

The interchange of radiation between the various volume and surface zones within the combustion chamber is determined by the Monte Carlo method, described in details by earlier authors [28–30]. The fraction of radiation emitted from any one zone and absorbed by any other zone was determined by this random paths technique. Although this procedure is time-consuming in computation time, it is in principle completely rigorous for the emitting, scattering and absorbing process.

2.2.2. Monte Carlo method for total interchange areas calculation

The Monte Carlo method is based on probability and statistics. The concept of energy bundle is introduced to simulate actual physical process of radiation [16]. A statistically meaningful number of energy bundles are followed from initial point of emission through randomly determined paths until the final point of absorption in the system.

The definition of total view factor f_{ij} is introduced which is the ratio of the number of bundles absorbed in zone "j" and originally emitted from zone "i", to the total number of bundles released from zone "i". The total interchange areas can be expressed in the following form:

$$\overline{S_jS_i} = A_j\varepsilon_j f_{ji} \tag{21}$$

$$\overline{G_kS_i} = 4K_kV_kf_{ki} \tag{22}$$

$$\overline{S_jG_i} = A_j\varepsilon_j f_{ji} \tag{23}$$

$$\overline{G_kG_i} = 4K_kV_kf_{ki} \tag{24}$$

The Total Interchange Areas (TIA), which have the dimension of area (L^2), are linked with Monte Carlo method through Total View Factors f_{ij} which are also called in some literature Total Interchange Factors (TIF).

The random paths are formulated by following randomly generated decisions. The cumulative distribution function $R(\xi)$ is taken to be a random number R_i. Once the random number R_i is generated, the required value for the appropriate variable ξ (which can be coordinates of the points, angles of direction, surface emissivities etc.) is calculated from the available relation $R(\xi)$.

Different cumulative distribution functions $R(\xi)$ are used for different variables, such as coordinates of the emission points, the angles determining the direction of emission, the maximum distance of travel etc. The methods of obtaining these cumulative distribution functions are presented in Refs. [11,16]. Every time a decision is necessary a random number in the interval 0.0–1.0 is generated.

The Monte Carlo relations used in the absence of solid particles are reported in Refs. [29,31,32].

The method adapted for the calculations of the radiative interchange involving the scattering by solid particles is reported in Refs. [30,33].

The cumulative distribution functions and basic equations used within Monte Carlo method, as well as the procedure related to energy bundle history are briefly presented in Appendix A.

3. Numerical characteristics

Two new different computer programs for the solution of 3-D RTE for the gray particles radiation are developed in this study. The Mie theory is incorporated in both. The first code is a combination of FVM and Mie theory. The

second code is based on the zone method where the total interchange areas are evaluated by Monte Carlo method. The second computer program consumes much more computer time and memory and was used here only to obtain the benchmark results for testing the first code.

The Mie theory has been incorporated in both methodologies used here, i.e. in (i) FVM coupled with Mie equations and in (ii) zone method linked with Monte Carlo technique. But it should be noticed that the conceptions of application of Mie theory in (i) and (ii) are completely different. In methodology (i), for various scattering angles the scattering phase functions were calculated to be used for the evaluation of scattered radiation energy within the process of solving RTE by FVM, i.e. to be used in Eq. (5) via Eq. (16). In methodology (ii), the angular distribution function, Eq. (A.8), in Appendix A, is set equal to the generated random number R_{11} for the sake of calculating the scattering angle α which is needed to define the direction of the scattered energy beam. The scattering angle α, together with angle β, defines the scattered direction which is necessary, using Eqs. (A.10) and (A.11), for the following the further history of the energy beam.

3.1. Numerical features of 3-D FVM coupled with Mie theory

A new original computer code that solves RTE for the gray particulate media in 3-D Cartesian coordinates based on FVM and coupled with Mie equations is developed. It is a modification of the previously developed 2-D code presented in Ref. [26]. Detailed and thorough discussion of finite volume method and of discretization procedure used in this work is given in literature [18–20] and it will not be discussed again. The spatial differencing scheme used in this work to relate the boundary intensities to nodal intensities is step scheme. This scheme sets the downstream boundary intensities equal to the upstream nodal intensities.

The iterative process of intensity calculation is repeated for all specified intensity directions and a solution is considered converged when it satisfies the following criterion:

$$|I_P^l - I_P^{l^0}|/I_P^l \leqslant 10^{-6} \tag{25}$$

Here I_P^l is the intensity calculated in the latest and $I_P^{l^0}$ the previous iteration.

The scheme appeared to be very efficient. The guess of initial intensity field is set to zero. The solution converges relatively fast. For the particular cases of anisotropic scattering in 3-D geometry where the particles cloud is considered as a gray medium, the incident heat flux is calculated with 11 iterations. But it should be noticed that, for 3-D geometry, within an iteration the code has eight sweeps, each of which in one of eight "vertex directions".

The cubical enclosure is subdivided into $15 \times 15 \times 15$ control volumes. The previous numerical experiments and analysis for this grid with the 3-D gray media [21] show that the results are grid independent.

The angular discretization has the number of increments in polar and azimuthal directions 12×20 respectively. The number of increments in polar and azimuthal directions of sub-control angles, within a control angle, is 3×3 respectively. Thus, the total number of solid sub-control angles, within a control angle, is taken $3 \times 3 = 9$ and is the same for both, incident and scattering directions.

The numerical experiments were performed by changing the number of solid sub-control angles. The subdivisions as 3×4, 3×5, 4×4, 4×5, 4×6 etc were carried out and it was found that these increases of sub-control angles did not influence on the accuracy.

For this FVM + ME code, the CPU time for the calculation cases performed here with 1.6 GHz Intel Pentium IV Processor with 256 KB Cache, having 1 GB (2*512 MB) 133 MHz non-ECC SDRAM of the work station designated as DELL optiplex GX240 is, depending on the case, about 4 min.

3.2. Numerical features of zone method linked with Monte Carlo method

Another code based on zone method, where total interchange factors were calculated by Monte Carlo method, was developed. It was done because the benchmark values, needed for comparison with the predictions of FVM + ME code, were not found in literature for these calculation cases.

For the sake of zone method implementation the considered geometry, that is the cube, is divided in 15 equal increments in each of the directions i.e. in x, y and z directions. It gives the total number of volume and surface zones 3375 and 1350 respectively. The total interchange factors (TIF-s) of radiative heat transfer were calculated using Monte Carlo method by emitting 50,000 energy bundles from each volume and surface zones. The numerical experiments with various numbers of energy bundles as with 10,000, 20,000, 50,000 and 100,000 were performed. It was found, for this particular case, that the number of 50,000 bundles gives the predictions which are not sensitive on further increasing of bundles number.

Related to Mie equations that were incorporated (but in different ways) in both codes, i.e. in (i) FVM + ME code and in (ii) ZM + MCM code, the following numerical features should be mentioned. For the designation "infinite refractive index" the value of 10^8 is taken. The larger values did not affect the results. Also for the definition of "very small particles" the value of $D_p = 0.01$ μm is taken, because the smaller values, (here is taken $\lambda = \pi$), i.e. for $x < 0.01$, did not influence on the predictions for function F2. The various infinite series within Mie equations were terminated for the value $n = 1.2x + 9$ where x is particle size parameter. This was proposed by Deirmendjian et al. [34].

For this ZM + MCM code, the CPU time for the calculation cases performed here with the same computer

mentioned above varies, depending on the case, between 14 and 16 min. Compared with 4 min taken by FV + ME, it was found that ZM + MC took from 3.5 to 4 times more the CPU time.

4. Calculation cases performed

The system geometry considered is a cube with side dimension 1.0 presented in Fig. 1. All six walls of the cube are black, i.e. for all of them $\varepsilon = 1$ and $\rho = 0$.

The walls are designated as west, east, south, north, rear and front having the subscripts w, e, s, n, r and f respectively. All the walls, as well as the medium in the enclosure, are kept cold and their emissive powers are $E_{bw} = E_{be} = E_{bs} = E_{bn} = E_{bf} = 0$. Only the rear wall is taken as a hot having constant emissive power $E_{br} = 1.0$. The enclosure contains pure scattering medium, i.e. for that medium the scattering albedo is equal to unity ($\omega = 1$), the absorption coefficient of medium (particles cloud) is equal to zero ($\kappa_p = 0$) and scattering coefficient is taken as unity ($\sigma = 1$). The quantities presented in this study are non-dimensional, i.e. normalized. The values as τ_x, τ_y and τ_z called optical coordinates and equal to βx, βy and βz respectively as well as the quantities as τ_{xL}, τ_{yL}, τ_{zL} designated as overall optical thicknesses and equal to βL are introduced. The relations between them as e.g. τ_x/τ_{xL} gives a non-dimensional coordinate $X = x/L$.

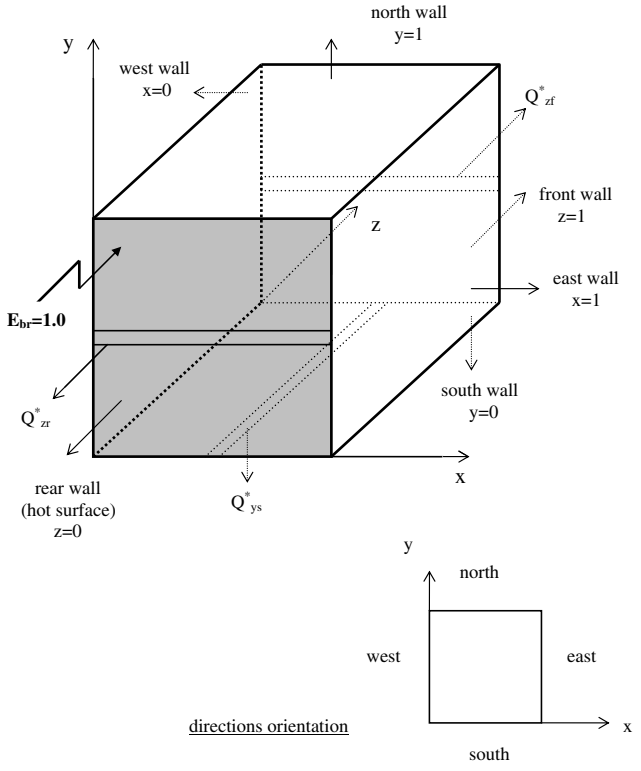

Fig. 1. System geometry.

Considering various particulate media, the predictions with both models, i.e. with (1) FV + ME and with (2) ZM + MC model, were carried out within this study. They are done for an isotropic medium, for four scattering phase functions (designated as F1, F2, B1 and B2) used by Kim and Lee [6] and Trivic et al. [26], as well as for a group of four different coals and an ash used in Ref. [26].

With capital letters F and B are indicated the scattering phase functions that have the peak values in forward and backward directions respectively. It means that from the total scattered energy backward scattering scatters more energy into the backward directions, while the forward scattering scatters more energy into the forward directions. The scattering phase functions F1, F2, B1 and B2 are presented and discussed in Refs. [6,15,18]. The data related to particles parameters for the definition of scattering phase functions F1, F2, B1 and B2 are presented in Table 1.

The dimensionless quantities that are calculated by both mathematical models are: (i) the net radiative heat flux in y-direction, Q^*_{ys}, at the middle of south wall ($X = 0.5$, $Y = 0.0$) along z-coordinate presented in Tables 3 and 4 and Fig. 2(a)–(c), (ii) the net radiative heat flux in z-direction, Q^*_{zr}, at the middle of rear, hot, wall ($Y = 0.5$, $Z = 0.0$) along x-coordinate presented in Tables 5 and 6 and Fig. 3(a)–(c), (iii) the net radiative heat flux in z-direction, Q^*_{zf}, at the middle of front, cold, wall ($Y = 0.5$, $Z = 1.0$) along x-coordinate presented in Tables 7 and 8 and Fig. 4(a)–(c), (iv) and the average incident radiation $G^*_z = G/4E$ along the centerline ($X = 0.5$, $Y = 0.5$) presented in Tables 9 and 10 and Fig. 5(a)–(c). Also the net radiative heat flux in z-direction $Q^*_z = Q_z/E$ along the centerline ($X = 0.5$, $Y = 0.5$) is calculated, but only with FV + ME, and presented in Table 11 and in Fig. 6(a). Here the z-direction is taken because the anisotropy of scattering phase functions plays important role in the radiative heat transfer when the boundary conditions are not symmetric. This is the case here in z-direction because the emissive

Table 1
Data for evaluation of scattering phase functions F1, F2, B1 and B2 by Mie equations

Scattering phase function designation	Particle size parameter $x = D_p\pi/\lambda$	Real part of complex index of refraction (absorptive index) n	Imaginary part of complex index of refraction (refractive index) k
F1	5	1.33	0
F2	2	1.33	0
B1	1	very large, taken 10^8	0
B2	D_p very small, taken $x = 0.01$	very large, taken 10^8	0

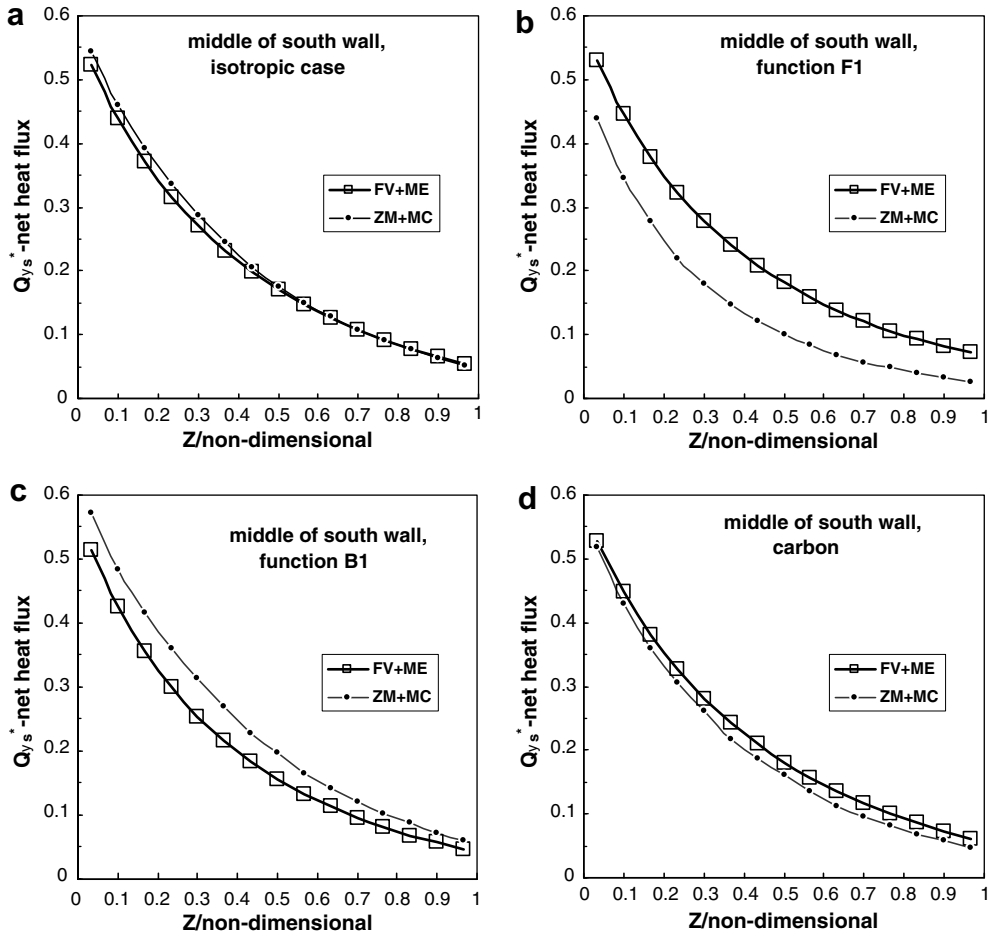

Fig. 2. Non-dimensional net radiative heat flux in y-direction, Q^*_{ys}, at the middle of south wall ($X = 0.5$, $Y = 0.0$) along z-coordinate predicted by FV + ME and by ZM + MC ($\rho = 0$, $\omega = 1$, $\sigma = 1$, $\kappa_p = 0$, cubical enclosure $1 \times 1 \times 1$): (a) isotropic scattering; (b) scattering phase function F1; (c) scattering phase function B1; (d) carbon.

power of rear wall is equal to unity and the emissive power of front wall is equal to zero. For the system with symmetric boundary conditions the effects of anisotropy are cancelled out to give isotropic results, regardless of anisotropy of the scattering phase functions involved. The net radiative heat flux in z-direction $Q^*_z = Q_z/E$ is evaluated as the difference of radiative heat flux in positive z-direction $Q^{+*}_z = Q^+_z/E$ and of radiative heat flux in negative z-direction $Q^{-*}_z = Q^-_z/E$.

It should be noticed that for the predictions where real fuels and an ash were analyzed, the geometry, the input parameters of the system ($\rho = 0$,$\omega = 1$,$\sigma = 1$, $\kappa_p = 0$) and all the boundary conditions (ρ, ε, E_{wb}, E_b) are the same as in previous calculation sets. Everything is the same except particles materials that are now: carbon, anthracite, bituminous, lignite and an ash. The data for evaluation of scattering phase functions for coals and ash considered related to near infrared region are taken from [11, Chap. 10], and is presented in Table 2. Instead of artificial media with anisotropic scattering, now the real engineering fuels are considered. The particle size parameters for all materials are taken as unity. It should be mentioned that here again, as in previous cases, particles concentrations and particles diameters are implicitly set or defined through chosen σ, κ_p, x and ω, and they are not explicitly expressed here.

5. Results and discussion

The curves for scattering phase functions (SPF-s) designated as F1, F2, B1 and B2 are presented in figures given in Refs. [6,18]. Also the SPF-s for four coals and ash, for the specified particles parameters, are given in figures shown in [26]. Therefore those figures will not be repeated here again. In this study the predictions were performed by both methods, i.e. by FV + ME and by ZM + MC, for all nine SPF-s as well as for isotropic scattering. For the sake of comparison with the results which will be calculated by other numerical methods and by other researchers, these sets of predictions are presented in Tables 3–11. In Figs. 2–5 are shown the comparisons between prediction obtained by two methods for isotropic scattering, phase functions F1, B1 and carbon. They are not given for functions F2, B2, anthracite, bituminous, lignite and ash. The following reasons are for that. It can be seen in

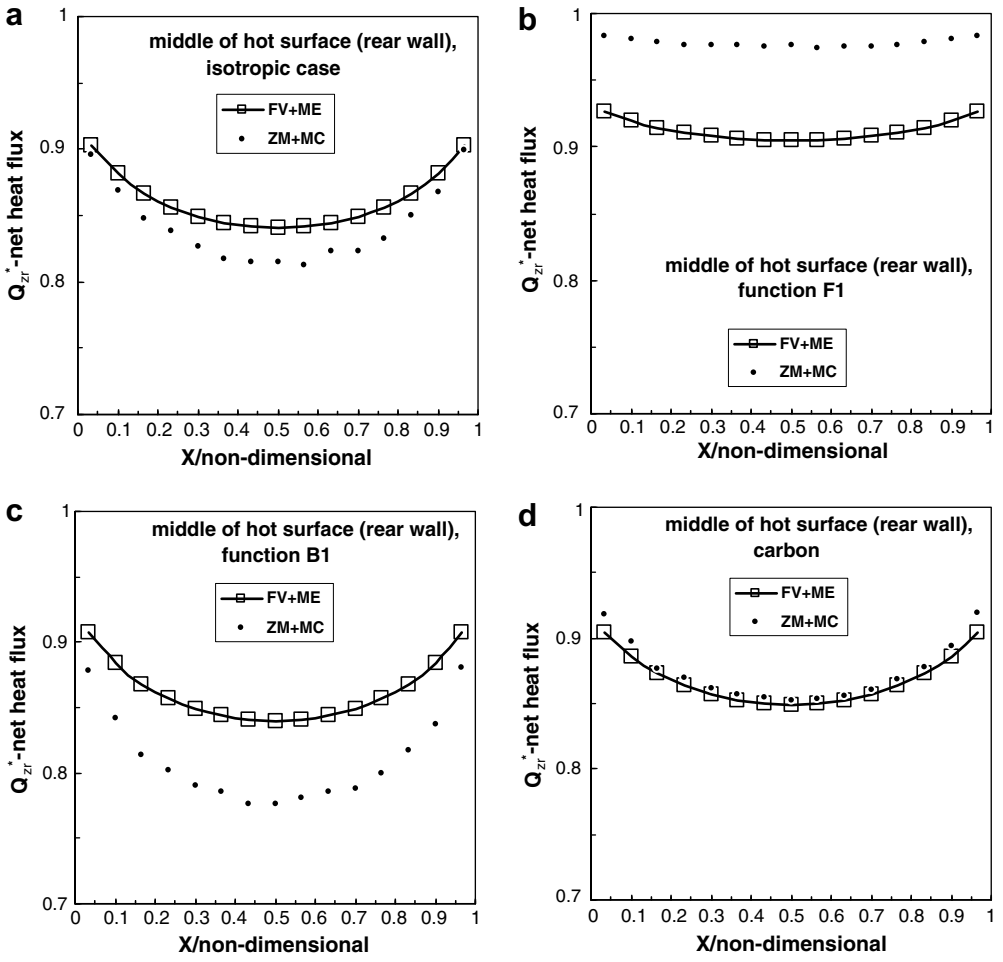

Fig. 3. Non-dimensional net radiative heat flux in z-direction, Q^*_{zr}, at the middle of rear, hot, wall ($Y = 0.5$, $Z = 0.0$) along x-coordinate predicted by FV + ME and by ZM + MC ($\rho = 0$, $\omega = 1$, $\sigma = 1$, $\kappa_p = 0$, cubical enclosure $1 \times 1 \times 1$): (a) isotropic scattering; (b) scattering phase function F1; (c) scattering phase function B1; (d) carbon.

Tables 3–11 that the predictions for phase functions F2 and B2 do not differ very much and are similar to predictions F1 and B1 respectively. Therefore, related to the comparison of predictions obtained by FV + ME and by ZM + MC, it was found that the results of analysis and the conclusions for F1 and B1 are the same and valid for F2 and B2 respectively. In Ref. [26] Trivic et al. have shown, in Fig. 2(a), the SPF-s for carbon, anthracite, bituminous, lignite and fly-ash. It was concluded there, that under the conditions considered, if the different particle materials (here the four coals and ash) have the same shape of scattering phase functions with small differences between them, it will result in the same values of net radiative heat flux and of average incident radiation for all those materials. In addition, it can be seen in Tables 3–11 that the predicted values of net radiative heat flux and of average incident radiation for carbon, anthracite, bituminous, lignite and ash are very close to each others. Therefore, under the conditions considered, whatever is found and concluded for carbon, it will be valid for anthracite, bituminous, lignite and ash. Thus there is no need to present and consider the graphs for these four materials and here only carbon was presented. Therefore in this study the predictions were carried out for nine scattering phase functions as well as for isotropic scattering, i.e. for 10 different cases, but only the four characteristic cases were analyzed.

The dimensionless net radiative heat flux, Q^*_z, in z-direction along the centerline ($X = 0.5$, $Y = 0.5$) for isotropic scattering, four different phase functions, four different coals and an ash predicted by Finite Volume Method and Mie theory is presented in Table 11. It should be mentioned that Q^*_z is not calculated by ZM + MC. The structure of developed ZM + MC model and code gives the net heat fluxes on the surroundings surfaces, but is not convenient for calculation of the net heat fluxes within the enclosure, i.e. out of the walls. For this purpose a new code should be developed, but it was not the goal of this study.

The more accurate results calculated by ZM + MC, therefore taken as benchmark, compared against FV + ME, can be, inter alia, explained in the following way. Using the large number, e.g. 50,000, energy beams released from each volume and surface zones, Monte Carlo

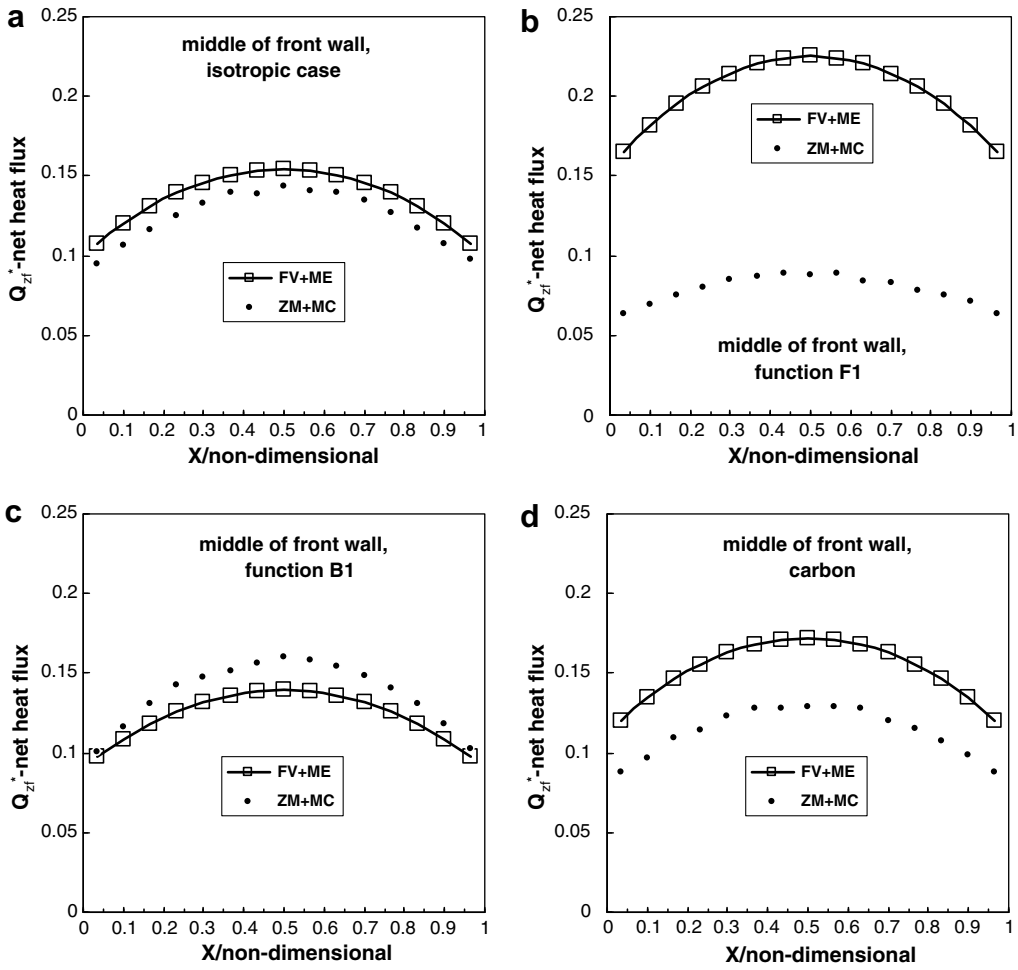

Fig. 4. Non-dimensional net radiative heat flux in z-direction, Q^*_{zf}, at the middle of front, cold, wall ($Y = 0.5$, $Z = 1.0$) along x-coordinate predicted by FV + ME and by ZM + MC ($\rho = 0$, $\omega = 1$, $\sigma = 1$, $\kappa_p = 0$, cubical enclosure $1 \times 1 \times 1$): (a) isotropic scattering; (b) scattering phase function F1; (c) scattering phase function B1; (d) carbon.

method has more efficient, i.e. superior mechanism of heat transfer than finite volume method. Within FV + ME the radiative heat is transferred via radiative intensities from a control volume. The number of the intensities is equal to the number of solid control angles, which is equal to the product of increments in polar and planar directions, e.g. here $6 \times 24 = 144$. This is always significantly less than the number of energy beams. Also the application of Monte Carlo method is a good example where a physical phenomenon, as radiation, is described by an adequate mathematical apparatus, here by Monte Carlo method. Monte Carlo technique intrinsically coincides with radiation and is more accurate by its own nature. On the other hand MC is numerically expensive procedure needing vast amount of computer time and memory, especially for complicated geometries and industrial modeling, and therefore is manly used for creating benchmark results.

In Fig. 2(a)–(d) the dimensionless net radiative heat flux in y-direction, Q^*_{ys}, at the middle of south wall, along z-coordinate, predicted by FV + ME and by ZM + MC for: (a) isotropic scattering; (b) scattering phase function F1; (c) scattering phase function B1 and (d) carbon are shown. In Fig. 2(a), i.e. for isotropic scattering, a good agreement between FV + ME predictions and ZM + MC values (taken as the benchmark) can be seen. In Fig. 2(b), where the phase function F1 is presented, the FV + ME values are higher, i.e. overestimated compared with benchmark. In Fig. 2(c), where the phase function B1 is shown, the FV + ME values are smaller, i.e. underestimated compared with benchmark. The FV + ME predictions shown in Fig. 2(d) for carbon, (carbon has the scattering phase function with a moderate forward character) are slightly overestimated. The trend is similar as for function F1.

In Fig. 3(a)–(d) the non-dimensional net radiative heat flux in z-direction, Q^*_{zr}, at the middle of rear, hot, wall along x-coordinate predicted by FV + ME and by ZM + MC for: (a) isotropic scattering; (b) phase function F1; (c) phase function B1 and (d) carbon are presented. Taking the ZM + MC predictions as the benchmark, the following results were found. In Fig. 3(a), where the isotropic scattering is considered, the FV + ME predictions are little overestimated. The FV + ME predictions for function F1, which are shown in Fig. 3(b), are to some extent

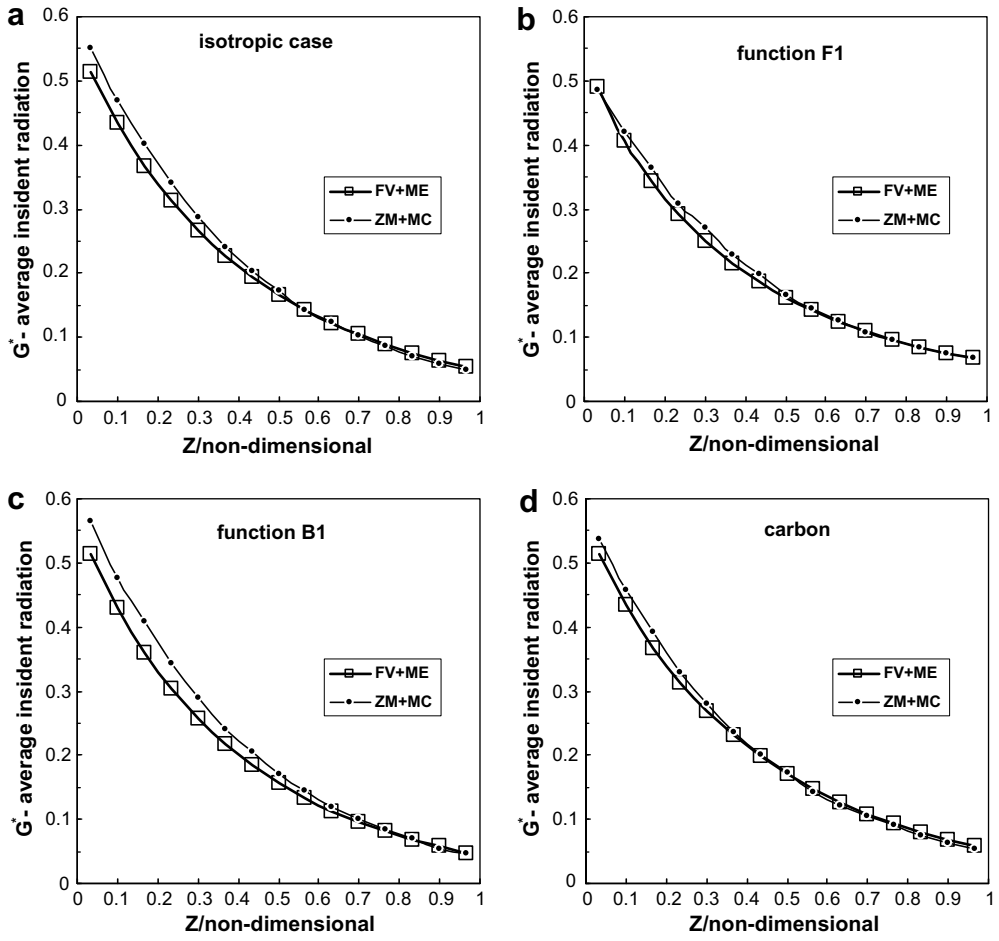

Fig. 5. Non-dimensional average incident radiation G^* along the centerline ($X = 0.5$, $Y = 0.5$) predicted by FV + ME and by ZM + MC ($\rho = 0$, $\omega = 1$, $\sigma = 1$, $\kappa_p = 0$, cubical enclosure $1 \times 1 \times 1$): (a) isotropic scattering; (b) scattering phase function F1; (c) scattering phase function B1; (d) carbon.

underestimated. These underestimations are between 5.7% and 7.3%. In Fig. 3(c), where function B1 is presented, the FV + ME results are overestimated from 2.9% to 7.6%. The FV + ME predictions presented in Fig. 3(d) for carbon show fairly good agreement with benchmark

In Fig. 4(a)–(d) the dimensionless net radiative heat flux in z-direction, Q^*_{zf}, at the middle of front, cold, wall along x-coordinate predicted by FV + ME and by ZM + MC for: (a) isotropic scattering; (b) function F1; (c) function B1 and (d) carbon are shown. Analyzing these figures the following was noticed. In Fig. 4(a), where the isotropic scattering is presented, the FV + ME results are slightly overestimated. The FV + ME predictions for function F1, shown in Fig. 4(b), are significantly overestimated. These overestimations are from 60.6% to 61.8%. In Fig. 4(c), where function B1 is presented, the FV + ME results are little underestimated. The FV + ME predictions presented in Fig. 4(d) for carbon are overestimated. These overestimations are from 24.9% to 27.2%.

In Fig. 5(a)–(d) the non-dimensional average incident radiation G^* along the centerline predicted by FV + ME and by ZM + MC for: (a) isotropic scattering; (b) phase function F1; (c) phase function B1 and (d) carbon are presented. It can be noticed fairly good agreement between FV + ME and ZM + MC predictions for all four cases, i.e. for isotropic scattering, functions F1 and B1 and carbon.

In Fig. 6(a)–(d) the effects of anisotropy for phase functions F1, F2, B1, B2, carbon and for isotropic scattering were shown by using FV + ME mathematical model and code. The net heat flux along the centerline, Q^*_z, in Fig. 6(a); the average incident radiation, G^*_z, in Fig. 6(b); the net heat flux on hot surface (rear wall), Q^*_{zr} in Fig. 6(c) and the net heat flux on cold surface (front wall), Q^*_{zf}, in Fig. 6(d) are presented. These graphs are given here, inter alia, for the sake of comparison and checking with the appropriate graphs shown in 2-D studies published in papers [6,26]. The curves in Fig. 6(a)–(d) have the same shapes and features and keep the same positions between themselves as the appropriate curves in [6,26]. They confirm the tendencies, findings and conclusions written in [6,26], and will not be presented again.

The graphs presented in Fig. 7(a)–(b) give the net heat flux, Q^*_z, along the center line for SPF F2. These curves show the sensitivity and flexibility of 3-D FV + ME model and code to the series of input data related to scattering

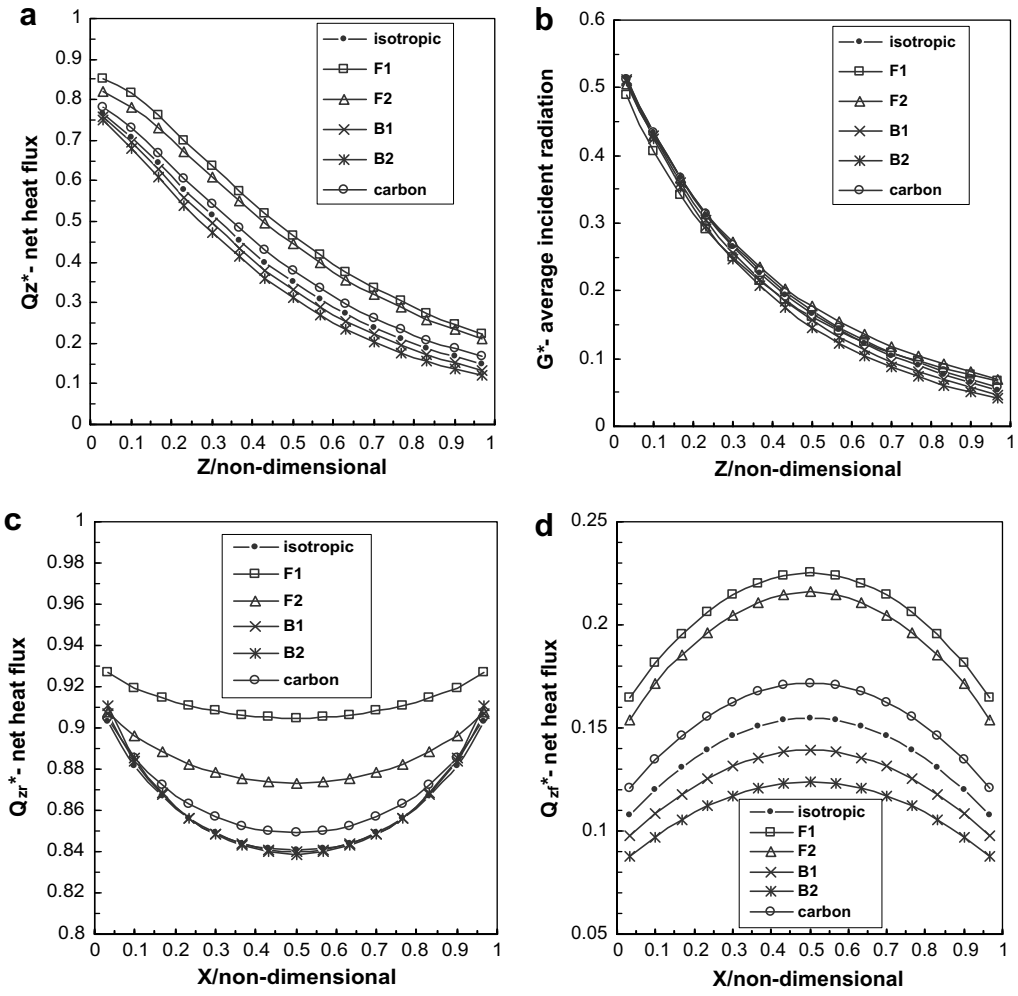

Fig. 6. Effects of anisotropy, predicted by FV + ME ($\rho = 0$, $\omega = 1$, $\sigma = 1$, $\kappa_p = 0$, cubical enclosure $1 \times 1 \times 1$) for four scattering phase functions, carbon and isotropic scattering related to: (a) non-dimensional net radiative heat flux in z-direction, Q_z^*, along the centerline ($X = 0.5$, $Y = 0.5$); (b) non-dimensional average incident radiation G^* along the centerline ($X = 0.5$, $Y = 0.5$); (c) non-dimensional net radiative heat flux in z-direction, Q_{zr}^*, at the middle of rear, hot, wall ($Y = 0.5$, $Z = 0.0$) along x-coordinate; (d) non-dimensional net radiative heat flux in z-direction, Q_{zf}^*, at the middle of front, cold, wall ($Y = 0.5$, $Z = 1.0$) along x-coordinate.

Table 2
Data of complex refractive index for different colas and an ash in near infrared region taken from [11] for the evaluation of scattering phase functions

Coal or ash	Particle size parameter $x = D_p\pi/\lambda$	Real part of complex index of refraction (absorptive index) n	Imaginary part of complex index of refraction (refractive index) k
Carbon	1	2.20	1.120
Anthracite	1	2.05	0.540
Bituminous	1	1.85	0.220
Lignite	1	1.70	0.066
Ash	1	1.50	0.020

albedo, ω, and to wall reflectivity, ρ respectively. The shape and the tendency of the curves, as well as their positions, are the same as it is for 2-D cases presented in [6,26]. Also the same effects of ω and ρ on Q_z^* is found as in 2-D cases [6,26] as well as the same conclusions can be drown and it will not be discussed again. Figs. 6(a)–(d) and 7(a)–(b) give an additional proof for the reliability of the 3-D FV + ME methodology.

It can be seen in Fig. 3(b) and (c) where the net heat flux on hot surface for phase functions F1 and B1 are presented respectively as well as in Fig. 4(b) where the net heat flux on the opposite i.e. cold surface for phase function F1 is shown, that the differences between FV + ME predictions and benchmark (ZM + MC results) are significant. It should be kept in mind that this is for scattering phase functions F1 and B1 which have the strong forward and

Table 3
Non-dimensional net radiative heat flux in y-direction, Q^*_{ys}, at the middle of south wall ($X = 0.5$, $Y = 0.0$) along z-coordinate for: isotropic scattering, four different phase functions, four different coals and an ash predicted by Finite Volume Method and Mie theory ($\rho = 0$, $\omega = 1$, $\sigma = 1$, $\kappa_p = 0$, cubical enclosure $1 \times 1 \times 1$)

Z	ISO	F1	F2	B1	B2	Carb.	Anth.	Bitu.	Lign.	Ash
0.0333	0.5224	0.5306	0.5414	0.5137	0.5046	0.5286	0.5311	0.5302	0.5290	0.5279
0.1000	0.4390	0.4469	0.4663	0.4267	0.4142	0.4477	0.4512	0.4501	0.4483	0.4468
0.1667	0.3704	0.3776	0.4020	0.3563	0.3420	0.3804	0.3845	0.3832	0.3811	0.3794
0.2333	0.3152	0.3225	0.3490	0.3002	0.2852	0.3259	0.3303	0.3288	0.3266	0.3248
0.3000	0.2698	0.2780	0.3046	0.2545	0.2394	0.2807	0.2852	0.2837	0.2815	0.2795
0.3667	0.2314	0.2407	0.2663	0.2163	0.2015	0.2423	0.2468	0.2453	0.2430	0.2411
0.4333	0.1986	0.2089	0.2329	0.1839	0.1697	0.2091	0.2136	0.2121	0.2099	0.2080
0.5000	0.1703	0.1817	0.2037	0.1564	0.1429	0.1805	0.1848	0.1834	0.1813	0.1795
0.5667	0.1461	0.1583	0.1783	0.1329	0.1204	0.1558	0.1599	0.1586	0.1565	0.1548
0.6333	0.1252	0.1383	0.1561	0.1130	0.1013	0.1345	0.1383	0.1371	0.1352	0.1335
0.7000	0.1072	0.1210	0.1367	0.0959	0.0853	0.1160	0.1196	0.1184	0.1166	0.1151
0.7667	0.0916	0.1061	0.1196	0.0813	0.0717	0.0998	0.1032	0.1021	0.1004	0.0990
0.8333	0.0779	0.0930	0.1044	0.0686	0.0600	0.0856	0.0887	0.0877	0.0861	0.0848
0.9000	0.0657	0.0816	0.0906	0.0574	0.0498	0.0728	0.0756	0.0747	0.0733	0.0721
0.9667	0.0544	0.0713	0.0776	0.0473	0.0408	0.0610	0.0635	0.0627	0.0614	0.0604

Table 4
Non-dimensional net radiative heat flux in y-direction, Q^*_{ys}, at the middle of south wall ($X = 0.5$, $Y = 0.0$) along z-coordinate for: isotropic scattering, four different phase functions, four different coals and an ash predicted by Zone and Monte Carlo method ($\rho = 0$, $\omega = 1$, $\sigma = 1$, $\kappa_p = 0$, cubical enclosure $1 \times 1 \times 1$)

Z	ISO	F1	F2	B1	B2	Carb.	Anth.	Bitu.	Lign.	Ash
0.0333	0.5450	0.4399	0.4529	0.5728	0.5951	0.5174	0.5086	0.5151	0.5194	0.5199
0.1000	0.4591	0.3453	0.3572	0.4847	0.5153	0.4296	0.4225	0.4251	0.4284	0.4320
0.1667	0.3912	0.2788	0.2825	0.4164	0.4506	0.3592	0.3531	0.3584	0.3594	0.3619
0.2333	0.3352	0.2200	0.2304	0.3596	0.3883	0.3061	0.2981	0.2951	0.3013	0.3077
0.3000	0.2865	0.1808	0.1878	0.3136	0.3410	0.2607	0.2511	0.2530	0.2579	0.2626
0.3667	0.2448	0.1474	0.1565	0.2705	0.2911	0.2179	0.2072	0.2136	0.2177	0.2208
0.4333	0.2059	0.1208	0.1268	0.2289	0.2540	0.1876	0.1771	0.1789	0.1837	0.1876
0.5000	0.1742	0.1004	0.1070	0.1979	0.2156	0.1612	0.1520	0.1551	0.1569	0.1605
0.5667	0.1504	0.0836	0.0858	0.1654	0.1893	0.1345	0.1248	0.1293	0.1349	0.1338
0.6333	0.1287	0.0674	0.0704	0.1427	0.1591	0.1120	0.1088	0.1114	0.1125	0.1157
0.7000	0.1083	0.0571	0.0609	0.1214	0.1366	0.0960	0.0919	0.0924	0.0953	0.0959
0.7667	0.0903	0.0480	0.0479	0.1021	0.1147	0.0818	0.0786	0.0802	0.0788	0.0841
0.8333	0.0770	0.0393	0.0408	0.0889	0.0978	0.0682	0.0654	0.0651	0.0666	0.0702
0.9000	0.0641	0.0327	0.0340	0.0722	0.0820	0.0578	0.0548	0.0542	0.0562	0.0579
0.9667	0.0521	0.0264	0.0286	0.0597	0.0642	0.0468	0.0433	0.0449	0.0454	0.0472

Table 5
Non-dimensional net radiative heat flux in z-direction, Q^*_{zr}, at the middle of rear, hot, wall ($Y = 0.5$, $Z = 0.0$) along x-coordinate for: isotropic scattering, four different phase functions, four different coals and an ash predicted by Finite Volume Method and Mie theory ($\rho = 0$, $\omega = 1$, $\sigma = 1$, $\kappa_p = 0$, cubical enclosure $1 \times 1 \times 1$)

X	ISO	F1	F2	B1	B2	Carb.	Anth.	Bitu.	Lign.	Ash
0.0333	0.9032	0.9266	0.9079	0.9070	0.9105	0.9043	0.9039	0.9041	0.9043	0.9046
0.1000	0.8815	0.9195	0.8963	0.8836	0.8853	0.8854	0.8858	0.8858	0.8856	0.8855
0.1667	0.8667	0.9144	0.8883	0.8676	0.8683	0.8725	0.8734	0.8732	0.8728	0.8724
0.2333	0.8564	0.9107	0.8825	0.8565	0.8565	0.8633	0.8646	0.8642	0.8636	0.8631
0.3000	0.8491	0.9081	0.8784	0.8487	0.8483	0.8568	0.8584	0.8579	0.8572	0.8566
0.3667	0.8442	0.9063	0.8756	0.8436	0.8429	0.8524	0.8542	0.8537	0.8529	0.8522
0.4333	0.8415	0.9053	0.8740	0.8407	0.8398	0.8499	0.8518	0.8513	0.8504	0.8497
0.5000	0.8406	0.9049	0.8734	0.8397	0.8388	0.8491	0.8510	0.8505	0.8496	0.8488
0.5667	0.8415	0.9053	0.8740	0.8407	0.8398	0.8499	0.8518	0.8513	0.8504	0.8497
0.6333	0.8442	0.9063	0.8756	0.8436	0.8429	0.8524	0.8542	0.8537	0.8529	0.8522
0.7000	0.8491	0.9081	0.8784	0.8487	0.8483	0.8568	0.8584	0.8579	0.8572	0.8566
0.7667	0.8564	0.9107	0.8825	0.8565	0.8565	0.8633	0.8646	0.8642	0.8636	0.8631
0.8333	0.8667	0.9144	0.8883	0.8676	0.8683	0.8725	0.8734	0.8732	0.8728	0.8724
0.9000	0.8815	0.9195	0.8963	0.8836	0.8853	0.8854	0.8858	0.8858	0.8856	0.8855
0.9667	0.9032	0.9266	0.9079	0.9070	0.9105	0.9043	0.9039	0.9041	0.9043	0.9046

Table 6
Non-dimensional net radiative heat flux in z-direction, Q^*_{zr}, at the middle of rear, hot, wall ($Y = 0.5$, $Z = 0.0$) along x-coordinate for: isotropic scattering, four different phase functions, four different coals and an ash predicted by Zone and Monte Carlo method ($\rho = 0$, $\omega = 1$, $\sigma = 1$, $\kappa_p = 0$, cubical enclosure $1 \times 1 \times 1$)

X	ISO	F1	F2	B1	B2	Carb.	Anth.	Bitu.	Lign.	Ash
0.0333	0.8957	0.9834	0.9690	0.8778	0.8624	0.9180	0.9248	0.9223	0.9206	0.9157
0.1000	0.8683	0.9802	0.9617	0.8421	0.8142	0.8969	0.9023	0.9008	0.8973	0.8926
0.1667	0.8480	0.9780	0.9603	0.8142	0.7832	0.8762	0.8906	0.8855	0.8812	0.8775
0.2333	0.8385	0.9760	0.9574	0.8016	0.7653	0.8699	0.8799	0.8767	0.8717	0.8695
0.3000	0.8265	0.9764	0.9573	0.7900	0.7542	0.8613	0.8758	0.8700	0.8625	0.8599
0.3667	0.8176	0.9763	0.9548	0.7854	0.7453	0.8568	0.8682	0.8641	0.8589	0.8531
0.4333	0.8143	0.9747	0.9539	0.7757	0.7378	0.8543	0.8677	0.8634	0.8583	0.8515
0.5000	0.8153	0.9761	0.9531	0.7757	0.7378	0.8527	0.8664	0.8623	0.8562	0.8477
0.5667	0.8125	0.9737	0.9537	0.7813	0.7398	0.8531	0.8696	0.8649	0.8565	0.8499
0.6333	0.8226	0.9756	0.9558	0.7860	0.7429	0.8562	0.8716	0.8629	0.8602	0.8523
0.7000	0.8229	0.9755	0.9573	0.7877	0.7523	0.8602	0.8742	0.8680	0.8617	0.8563
0.7667	0.8319	0.9763	0.9576	0.7999	0.7680	0.8689	0.8790	0.8752	0.8666	0.8615
0.8333	0.8498	0.9781	0.9593	0.8177	0.7859	0.8775	0.8913	0.8841	0.8780	0.8749
0.9000	0.8680	0.9802	0.9628	0.8376	0.8141	0.8937	0.9041	0.9016	0.8958	0.8890
0.9667	0.8991	0.9835	0.9689	0.8800	0.8611	0.9194	0.9241	0.9211	0.9195	0.9159

Table 7
Non-dimensional net radiative heat flux in z-direction, Q^*_{zf}, at the middle of front wall ($Y = 0.5$, $Z = 1.0$) along x-coordinate for: isotropic scattering, four different phase functions, four different coals and an ash predicted by Finite Volume Method and Mie theory ($\rho = 0$, $\omega = 1$, $\sigma = 1$, $\kappa_p = 0$, cubical enclosure $1 \times 1 \times 1$)

X	ISO	F1	F2	B1	B2	Carb.	Anth.	Bitu.	Lign.	Ash
0.0333	0.1075	0.1649	0.1538	0.0975	0.0876	0.1206	0.1247	0.1234	0.1214	0.1197
0.1000	0.1201	0.1817	0.1712	0.1086	0.0971	0.1345	0.1392	0.1378	0.1355	0.1335
0.1667	0.1307	0.1952	0.1853	0.1180	0.1053	0.1461	0.1512	0.1496	0.1471	0.1450
0.2333	0.1393	0.2060	0.1964	0.1255	0.1120	0.1554	0.1608	0.1591	0.1565	0.1542
0.3000	0.1459	0.2143	0.2049	0.1314	0.1172	0.1626	0.1682	0.1664	0.1637	0.1613
0.3667	0.1507	0.2203	0.2110	0.1357	0.1209	0.1677	0.1735	0.1717	0.1689	0.1665
0.4333	0.1536	0.2239	0.2147	0.1383	0.1232	0.1709	0.1767	0.1749	0.1720	0.1696
0.5000	0.1545	0.2251	0.2159	0.1392	0.1240	0.1719	0.1778	0.1759	0.1731	0.1706
0.5667	0.1536	0.2239	0.2147	0.1383	0.1232	0.1709	0.1767	0.1749	0.1720	0.1696
0.6333	0.1507	0.2203	0.2110	0.1357	0.1209	0.1677	0.1735	0.1717	0.1689	0.1665
0.7000	0.1459	0.2143	0.2049	0.1314	0.1172	0.1626	0.1682	0.1664	0.1637	0.1613
0.7667	0.1393	0.2060	0.1964	0.1255	0.1120	0.1554	0.1608	0.1591	0.1565	0.1542
0.8333	0.1307	0.1952	0.1853	0.1180	0.1053	0.1461	0.1512	0.1496	0.1471	0.1450
0.9000	0.1201	0.1817	0.1712	0.1086	0.0971	0.1345	0.1392	0.1378	0.1355	0.1335
0.9667	0.1075	0.1649	0.1538	0.0975	0.0876	0.1206	0.1247	0.1234	0.1214	0.1197

Table 8
Non-dimensional net radiative heat flux in z-direction, Q^*_{zf}, at the middle of front wall ($Y = 0.5$, $Z = 1.0$) along x-coordinate for: isotropic scattering, four different phase functions, four different coals and an ash predicted by Zone and Monte Carlo method ($\rho = 0$, $\omega = 1$, $\sigma = 1$, $\kappa_p = 0$, cubical enclosure $1 \times 1 \times 1$)

X	ISO	F1	F2	B1	B2	Carb.	Anth.	Bitu.	Lign.	Ash
0.0333	0.0946	0.0630	0.0664	0.1010	0.1094	0.0877	0.0862	0.0854	0.0867	0.0895
0.1000	0.1066	0.0695	0.0724	0.1163	0.1275	0.0969	0.0941	0.0958	0.0960	0.1001
0.1667	0.1159	0.0755	0.0761	0.1308	0.1418	0.1091	0.1020	0.1046	0.1072	0.1065
0.2333	0.1250	0.0802	0.0805	0.1422	0.1537	0.1138	0.1123	0.1134	0.1146	0.1169
0.3000	0.1328	0.0846	0.0834	0.1473	0.1632	0.1226	0.1160	0.1154	0.1210	0.1239
0.3667	0.1393	0.0870	0.0866	0.1509	0.1715	0.1275	0.1197	0.1229	0.1262	0.1267
0.4333	0.1389	0.0885	0.0896	0.1565	0.1765	0.1283	0.1240	0.1232	0.1274	0.1318
0.5000	0.1431	0.0881	0.0893	0.1597	0.1752	0.1290	0.1228	0.1249	0.1269	0.1325
0.5667	0.1404	0.0886	0.0882	0.1581	0.1744	0.1287	0.1207	0.1231	0.1294	0.1295
0.6333	0.1393	0.0844	0.0843	0.1544	0.1706	0.1281	0.1210	0.1242	0.1254	0.1263
0.7000	0.1351	0.0833	0.0832	0.1480	0.1596	0.1198	0.1168	0.1191	0.1196	0.1244
0.7667	0.1268	0.0778	0.0806	0.1408	0.1566	0.1148	0.1099	0.1139	0.1165	0.1152
0.8333	0.1171	0.0749	0.0741	0.1313	0.1414	0.1070	0.1032	0.1030	0.1047	0.1091
0.9000	0.1070	0.0715	0.0724	0.1184	0.1270	0.0987	0.0942	0.0944	0.0962	0.1011
0.9667	0.0972	0.0638	0.0665	0.1027	0.1101	0.0878	0.0820	0.0836	0.0880	0.0858

Table 9
Non-dimensional average incident radiation G^* along the centerline ($X = 0.5,\ Y = 0.5$) for: isotropic scattering, four different phase functions, four different coals and an ash predicted by Finite Volume Method and Mie theory ($\rho = 0$, $\omega = 1$, $\sigma = 1$, $\kappa_p = 0$, cubical enclosure $1 \times 1 \times 1$)

Z	ISO	F1	F2	B1	B2	Carb.	Anth.	Bitu.	Lign.	Ash
0.0333	0.5142	0.4903	0.5065	0.5125	0.5103	0.5128	0.5127	0.5127	0.5128	0.5128
0.1000	0.4333	0.4073	0.4294	0.4286	0.4235	0.4331	0.4336	0.4334	0.4331	0.4329
0.1667	0.3669	0.3426	0.3664	0.3600	0.3527	0.3677	0.3688	0.3684	0.3678	0.3673
0.2333	0.3123	0.2919	0.3150	0.3040	0.2953	0.3140	0.3155	0.3150	0.3142	0.3136
0.3000	0.2664	0.2503	0.2718	0.2572	0.2476	0.2688	0.2706	0.2700	0.2691	0.2683
0.3667	0.2273	0.2157	0.2350	0.2177	0.2077	0.2304	0.2323	0.2317	0.2306	0.2298
0.4333	0.1941	0.1866	0.2038	0.1843	0.1743	0.1976	0.1998	0.1990	0.1979	0.1970
0.5000	0.1660	0.1621	0.1772	0.1562	0.1464	0.1698	0.1720	0.1713	0.1701	0.1692
0.5667	0.1420	0.1415	0.1545	0.1325	0.1230	0.1461	0.1484	0.1476	0.1465	0.1455
0.6333	0.1216	0.1239	0.1351	0.1125	0.1035	0.1259	0.1281	0.1274	0.1262	0.1253
0.7000	0.1040	0.1090	0.1184	0.0954	0.0870	0.1085	0.1107	0.1100	0.1089	0.1079
0.7667	0.0889	0.0961	0.1039	0.0809	0.0730	0.0935	0.0956	0.0949	0.0938	0.0929
0.8333	0.0757	0.0850	0.0912	0.0683	0.0611	0.0803	0.0824	0.0817	0.0807	0.0798
0.9000	0.0639	0.0754	0.0799	0.0572	0.0507	0.0686	0.0706	0.0700	0.0690	0.0681
0.9667	0.0532	0.0668	0.0697	0.0472	0.0415	0.0579	0.0598	0.0592	0.0582	0.0574

Table 10
Non-dimensional average incident radiation G^* along the centerline ($X = 0.5,\ Y = 0.5$) for: isotropic scattering, four different phase functions, four different coals and an ash predicted by Zone and Monte Carlo method ($\rho = 0$, $\omega = 1$, $\sigma = 1$, $\kappa_p = 0$, cubical enclosure $1 \times 1 \times 1$)

Z	ISO	F1	F2	B1	B2	Carb.	Anth.	Bitu.	Lign.	Ash
0.0333	0.5515	0.4845	0.4907	0.5647	0.5788	0.5366	0.5257	0.5316	0.5368	0.5378
0.1000	0.4684	0.4214	0.4222	0.4759	0.4937	0.4571	0.4538	0.4524	0.4558	0.4591
0.1667	0.4020	0.3645	0.3667	0.4082	0.4168	0.3925	0.3867	0.3865	0.3924	0.3885
0.2333	0.3409	0.3088	0.3179	0.3443	0.3524	0.3298	0.3279	0.3274	0.3261	0.3302
0.3000	0.2869	0.2698	0.2682	0.2901	0.2916	0.2804	0.2768	0.2814	0.2795	0.2796
0.3667	0.2403	0.2279	0.2304	0.2416	0.2416	0.2363	0.2367	0.2358	0.2373	0.2371
0.4333	0.2035	0.1976	0.1945	0.2059	0.2049	0.1999	0.1987	0.1982	0.1988	0.1998
0.5000	0.1723	0.1657	0.1691	0.1714	0.1698	0.1716	0.1683	0.1683	0.1708	0.1712
0.5667	0.1423	0.1437	0.1465	0.1437	0.1412	0.1424	0.1453	0.1432	0.1454	0.1424
0.6333	0.1226	0.1268	0.1272	0.1184	0.1165	0.1218	0.1216	0.1250	0.1206	0.1222
0.7000	0.1036	0.1075	0.1131	0.1009	0.0984	0.1046	0.1052	0.1019	0.1054	0.1047
0.7667	0.0868	0.0952	0.0971	0.0847	0.0815	0.0900	0.0888	0.0893	0.0888	0.0889
0.8333	0.0712	0.0851	0.0863	0.0697	0.0662	0.0749	0.0770	0.0774	0.0769	0.0741
0.9000	0.0586	0.0751	0.0740	0.0545	0.0557	0.0636	0.0664	0.0656	0.0650	0.0648
0.9667	0.0488	0.0678	0.0676	0.0470	0.0422	0.0536	0.0543	0.0551	0.0517	0.0549

Table 11
Non-dimensional net radiative heat flux, Q_z^*, in z-direction along the centerline ($X = 0.5,\ Y = 0.5$) for: isotropic scattering, four different phase functions, four different coals and an ash predicted by Finite Volume Method and Mie theory ($\rho = 0$, $\omega = 1$, $\sigma = 1$, $\kappa_p = 0$, cubical enclosure $1 \times 1 \times 1$)

Z	ISO	F1	F2	B1	B2	Carb.	Anth.	Bitu.	Lign.	Ash
0.0333	0.7661	0.8523	0.8219	0.7580	0.7491	0.7820	0.7862	0.7850	0.7829	0.7812
0.1000	0.7075	0.8162	0.7817	0.6951	0.6815	0.7292	0.7351	0.7333	0.7305	0.7281
0.1667	0.6431	0.7626	0.7290	0.6276	0.6105	0.6685	0.6755	0.6734	0.6700	0.6672
0.2333	0.5774	0.7011	0.6702	0.5598	0.5405	0.6050	0.6127	0.6104	0.6067	0.6035
0.3000	0.5138	0.6377	0.6098	0.4948	0.4742	0.5423	0.5504	0.5480	0.5441	0.5407
0.3667	0.4544	0.5760	0.5510	0.4347	0.4136	0.4830	0.4913	0.4888	0.4848	0.4813
0.4333	0.4003	0.5183	0.4957	0.3804	0.3594	0.4285	0.4367	0.4342	0.4302	0.4268
0.5000	0.3519	0.4655	0.4448	0.3323	0.3117	0.3792	0.3873	0.3848	0.3809	0.3775
0.5667	0.3092	0.4177	0.3986	0.2901	0.2701	0.3354	0.3432	0.3408	0.3370	0.3337
0.6333	0.2717	0.3750	0.3573	0.2533	0.2342	0.2967	0.3042	0.3019	0.2982	0.2951
0.7000	0.2392	0.3369	0.3204	0.2216	0.2034	0.2627	0.2699	0.2677	0.2642	0.2612
0.7667	0.2111	0.3032	0.2878	0.1943	0.1771	0.2332	0.2400	0.2379	0.2346	0.2317
0.8333	0.1870	0.2734	0.2590	0.1710	0.1548	0.2076	0.2141	0.2121	0.2090	0.2062
0.9000	0.1665	0.2470	0.2339	0.1512	0.1359	0.1857	0.1918	0.1899	0.1869	0.1843
0.9667	0.1491	0.2238	0.2121	0.1345	0.1200	0.1669	0.1727	0.1709	0.1681	0.1656

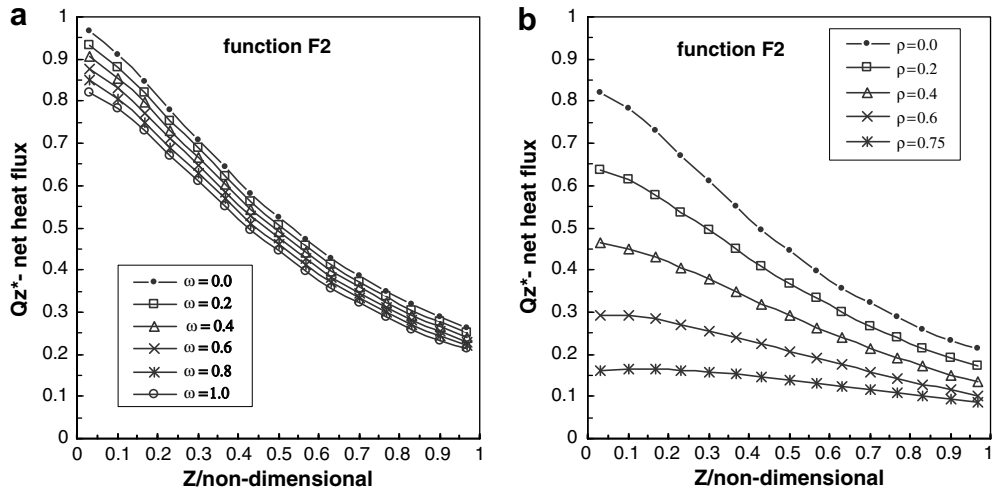

Fig. 7. Influence of scattering albedo and of wall reflectivity on non-dimensional net radiative heat flux in z-direction, Q_z^*, along the centerline ($X = 0.5$, $Y = 0.5$) predicted by FV + ME ($\rho = 0$, $\omega = 1$, $\sigma = 1$, $\kappa_p = 0$, cubical enclosure $1 \times 1 \times 1$) for scattering phase function F2: (a) effect of scattering albedo on Q_z^*; (b) effect of wall reflectivity on Q_z^*.

backward characters respectively. All other differences between FV + ME and ZM + MC predictions, especially for four coals and ash, presented in other figures, are moderate. Fortunately, the mineral solid fuels, i.e. the majority of pulverized coals applied in industry as well as the ash particles created there, under the conditions and with particles parameters used in combustion systems have the scattering phase functions with moderate forward features. It was found in Ref. [26] that scattering phase functions for carbon, anthracite, bituminous, lignite and ash, under the conditions considered, very little differ between themselves and that consequently the all predictions for these four coals and ash also very little differ between themselves. In addition it was found within this study that the agreement between FV + ME and ZM + MC predictions for carbon is good and it means the same for anthracite, bituminous, lignite and ash.

The explanation should be given for differences between FV + ME and ZM + MC predictions appeared in Fig. 3(b), (c) and 4(b). It can be seen in tables as well as in figures that FV + ME predictions for phase functions F1 and B1 compared with ZM + MC results are closer to isotropic predictions. The reason is because the FV + ME mathematical model does not have so efficient mechanism of radiation transfer as it is the case with Monte Carlo method that is discussed above in more details. The FV + ME model does not transfer so effectively the forward and backward features of phase functions F1 and B1 respectively as it is the case with ZM + MC methodology. Therefore the net radiative heat flux and the average incident radiation presented by FV + ME method have or "keep" more the isotropic character.

In Figs. 3(a)–(d) and 4(a)–(d) can be noticed a small asymmetry for ZM + MC results. It is known that the Monte Carlo predictions approach and fluctuate around the "exact" solutions as the number of emitted energy beams is increased. In this study, in spite the fact that 50,000 energy beams were released from each volume and surface zone and even for 100,000 energy beams, a mild asymmetry or results fluctuation appear. The reason for that is the "quality" of random number generator, i.e. how much the generated random numbers are really random.

In general, although not so accurate as Monte Carlo method, the finite volume method is numerically elegant and convenient for operation. Fortunately in many cases, especially for radiation modeling in industry, FVM is sufficiently accurate.

To the authors' best knowledge the methodology based on the link of 3-D finite volume method with Mie theory for anisotropic scattering of particulate media has not been developed before. In addition, the authors were not able to find in literature any results calculated by other methods to compare their 3-D predictions. The predictions obtained by FV + ME and by ZM + MC and presented in all figures and tables in this study are given, inter alia, to be compared against the results which will be predicted with other numerical methods. In this way these results will be objected or confirmed.

6. Conclusions

1. A new mathematical model and computer code for radiation of gray particulate media in 3-D rectangular enclosures based on coupling of FVM with Mie theory is developed. The physical and mathematical concepts of the model are presented. To the authors' best knowledge this methodology was not developed before. The series of predictions, related to net radiative heat flux and average incident radiation, were performed for: isotropic

scattering, four different scattering phase functions as well as for carbon, anthracite, bituminous, lignite and ash, i.e. altogether for ten various cases.

2. The 3-D benchmark needed for comparison, obtained previously by other methods or authors, either by experiments or by modeling, is missing in literature so far. Therefore another new model and code based on a combination of Zone Method with Monte Carlo Method were developed for generating benchmark results. With this model and code, for the sake of comparison, the benchmarks were calculated for the same ten cases as it was done with FV + ME method.
3. It was found that as far as the scattering phase functions are not very "exotic", i.e. as far as they do not have very strong forward or backward characters, which is not the case for usual industrial pulverized fuels under the conditions and with particles parameters used in the majority of combustion systems, the developed FV + ME mathematical model and code can be used with confidence in radiation modeling.
4. If the scattering phase functions express strong forward or backward characters, the FV + ME methodology will give the results which will significantly differ from "exact" solution. In these cases, to obtain the better accuracy, the ZM + MC methodology or another method should be applied.
5. The FV + ME mathematical model and code developed here show the following features: (i) reliably work in very wide, i.e. in all regions of various input data which take place within radiation and combustion problems; (ii) give, for coals, ash and radiation modeling in industry, good agreement with benchmark, i.e. sufficiently accurate predictions; (iii) can be applied for broad domain of particulate media needing only the particles diameters, density of particles material and complex index of refraction, i.e. work without the need for the design of the approximate analytical expressions for scattering phase functions.
6. The methodology developed and validated here can be further advanced towards: (i) incorporation in CFD codes, (ii) 3-D non-gray particulate media with anisotropic scattering, (iii) 3-D mixtures of non-gray gases and gray particles with anisotropic scattering, (iv) 3-D mixtures of non-gray gases and non-gray particles with anisotropic scattering and (v) incorporation of (ii), (iii) and (iv) in CFD codes.

Acknowledgments

A part of this study related to the mathematical model and code for 3-D finite volume method for particles radiation and its link with Mie theory was started in year 2002 within Institute for Complex Engineered Systems (ICES), Carnegie Mellon University (CMU), Pittsburgh, PA. The financial support for that part was provided by the US Department of Energy (DOE), National Energy Technology Laboratory (NETL), Morgantown, WV, within the Radiation Project for year 2002. D.N. Trivic wishes to thank Cristina H. Amon, former director of ICES and nowadays Dean of Faculty of Applied Science and Engineering, University of Toronto, for working within ICES and CMU. As a scientist her ideas are challenging and far-seeing. As a person she is very nice. It was a privilege working with her.

Appendix A. The energy bundle history in absorbing, emitting and scattering media

The cumulative distribution functions and basic equations used within Monte Carlo method, as well as the procedure related to energy bundle history are summarized below.

For the Monte Carlo method the radiation beams are simulated by energy bundles. A prescribed, statistically meaningful number of energy bundles are released from each volume and surface zone. The history of each bundle is followed until its final point of absorption.

(1) Coordinates of the emission points

For 3-D rectangular geometry three random numbers are generated as R_1, R_2 and R_3 and the coordinates of emission points x, y and z calculated by

$$x = (i-1)\Delta x + R_1\Delta x \tag{A.1}$$

$$y = (j-1)\Delta y + R_2\Delta y \tag{A.2}$$

$$z = (k-1)\Delta z + R_3\Delta z \tag{A.3}$$

where i, j and k are indices of the zones and Δx, Δy and Δz the dimensions of the zones. In the case of a surface zone one of these three coordinates is fixed by the location of that surface zone.

(2) Direction of emission

The random choices of polar angle η and planar angle θ specify the direction of the emitted bundle. Therefore the random numbers R_4, R_5 and R_6 are generated.

For emission from a volume zone polar angle η is calculated by

$$\cos\eta = 1 - 2R_4 \tag{A.4}$$

For emission or reflection from a diffuse surface the angle η is evaluated by

$$\cos^2\eta = 1 - R_5 \tag{A.5}$$

The planar angle for both cases, emission from a volume and from a surface zone is given by

$$\theta = 2\pi R_6 \tag{A.6}$$

It should be noticed that here, in Monte Carlo method, the polar and planar angles are designated as η and θ respectively. Within Finite Volume Method, in Section 2.1.1, the polar and planar angles are designated as θ and ϕ respectively. (Therefore angle θ in Monte Carlo calculations is planar angle, while in FVM is polar an-

gle.) This notation is kept in this study not only from historical reasons and because it is usual in literature, but also to emphasize the different ways of their calculations within these two various numerical methods.

(3) Maximum distance of travel in medium
The maximal distance of travel in the absorbing medium of uniform concentration of absorbing species is

$$L = -(\ln R_8)/K \tag{A.7}$$

(4) Final point of absorption of the bundle
Knowing the maximal distance and direction defined by the angles η and θ, the coordinates of the final points can be calculated from the geometrical relations. The final point of absorption can be inside, outside or exactly at the wall of the enclosure.If the final point is found to be outside the enclosure, it means this bundle must strike the wall. Another random number, R_9, is generated and compared to the surface absorptivity. When this random number is grater than the surface absorptivity, the bundle is reflected. The final coordinates of that bundle now become its initial coordinates. The direction of reflection is found by Eqs. (A.5) and (A.6), and the bundle followed thereon. If the random number R_9 is less than the surface absorptivity, the bundle is absorbed at the point and its history ends.When the final point of absorption of the bundle is within the enclosure, another random number, R_{10}, is generated and compared to the scattering albedo ω, of that gray gas. If the random number R_{10} is grater than the scattering albedo, the bundle is absorbed by the medium at that point and its history ends. In the case when the random number R_{10} is less than the scattering albedo, this bundle is scattered by solid particles. The final coordinates of that bundle now become its initial coordinates. Here the angular distribution function $f(\alpha)$, should be introduced which definition follows under (6). The next random number, R_{11}, is generated and the cumulative distribution function of the angular distribution function, $f(\alpha)$, is set equal to R_{11}, as follows:

$$R_{11} = \frac{\int_0^{\alpha} f(\alpha')\sin\alpha'\,\mathrm{d}\alpha'}{\int_0^{\pi} f(\alpha')\sin\alpha'\,\mathrm{d}\alpha'} \tag{A.8}$$

In such a way the scattering angle α, is evaluated. It is assumed that the radiation is not polarized after scattering. The angle between plane of incident beam and plane of scattered beam β is evaluated by generating the next random number, R_{12}, and using the relation:

$$\beta = 2\pi R_{12} \tag{A.9}$$

The direction of the scattered bundle defined by angles α and β is in a different coordinate system. This direction is transformed into the original coordinate system by using the relations:

$$\cos\eta_s = \cos\alpha\cos\eta + \sin\alpha\sin\eta\cos\beta \tag{A.10}$$

$$\cos(\theta_s - \theta) = \frac{\cos\alpha - \cos\eta\cos\eta_s}{\sin\eta\sin\eta_s} \tag{A.11}$$

More details on these trigonometric relations and their derivations with the pictures can be found in Ref. [33].The scattered bundle whose direction is defined in the original coordinate system is followed through all scatters and reflections until its final point of absorption.Once all the bundles have been released and followed to their final points of absorption, the bundles absorbed by each zone can be counted. The required quantity is the total view factor, f_{ij}, defined as the ratio of the number of bundles absorbed by the zone "j" which are released from the zone "i", to the total number of bundles released from the zone "i".

(5) Information on cumulative distribution functions used
Here should be mentioned that Chapter 19 of Ref. [11] gives the definition and discussion of cumulative distribution functions for Eqs. (A.1)–(A.3).
The data on other cumulative distribution functions are as follows. If the each of Eqs. (A.4)–(A.7) is solved for random numberR_i, i.e. written in the form as it is e.g. Eq. (A.4) as

$$R_4 = \frac{1-\cos\eta}{2} \tag{A.12}$$

and the same is done for Eqs. (A.5)–(A.7), then the expressions on the right hand side for, in this way written, all these four Eqs. (A.4)–(A.7) are the cumulative distribution functions. They are used for the calculation of required values as η, θ and L. The detailed derivation and discussion of these cumulative distribution functions are presented in Chapter 19 of Ref. [11].

(6) Definition of angular distribution function
The angular distribution function $f(\alpha)$, which is defined as the fraction of the scattered energy directed into a unit solid angle in the direction of the scattered angle α, measured from the forward direction, is given as

$$f(\alpha) = \frac{i_1 + i_2}{2\pi x^2 Q_{\mathrm{sca}}} \tag{A.13}$$

It should be mentioned that the same scattering angle is designated in this study with two different Greek letters: γ which comes from Mie theory notation in Eq. (14), and α used within Monte Carlo technique in Eqs. (A.8) and (A.13).The integration of the angular distribution function over the total solid angle gives

$$\int_0^{2\pi}\int_0^{\pi} f(\alpha)\sin\alpha\mathrm{d}\alpha\mathrm{d}\beta = 1.0 \tag{A.14}$$

One of the links between Monte Carlo method, i.e. (A.13), and Mie theory, i.e. Eq. (14) in Section 2.1.4, is that the angular distribution function, $f(\alpha)$, is given by

$$f(\alpha) = \frac{\Phi(\gamma)}{4\pi} \tag{A.15}$$

It is obvious that the angular distribution function is actually the scattering phase function divided by 4π.

References

[1] A.C. Ratzel III, J.R. Howell, Two-dimensional radiation in absorbing–emitting–scattering media using P-N approximation, ASME Paper 82-HT-19 (1982).

[2] W.A. Fiveland, Discrete-ordinates solutions of the radiative transport equation for rectangular enclosures, J. Heat Transfer 106 (1984) 699–706.

[3] A.L. Crosbie, R.G. Schrenker, Multiple scattering in two-dimensional rectangular medium exposed to collimated radiation, J. Quantit. Spectrosc. Radiat. Transfer 33 (2) (1985) 101–125.

[4] M.P. Menguc, R. Viscanta, Radiative transfer in three-dimensional rectangular enclosures containing inhomogeneous, anisotropically scattering media, J. Quantit. Spectrosc. Radiat. Transfer 33 (6) (1985) 533–549.

[5] S.T. Thynell, M.N. Ozisik, Radiation transfer in isotropically scattering rectangular enclosures, J. Thermophys. 1 (1) (1987) 69–76.

[6] T.K. Kim, H. Lee, Effect of anisotropic scattering on radiative heat transfer in two-dimensional enclosures, Int. J. Heat Mass Transfer 31 (8) (1988) 1711–1721.

[7] D.N. Trivic, Mathematical modeling of three-dimensional turbulent flow with combustion and radiation, Ph.D. Thesis, Department of Chemical Engineering, University of New Brunswick, Fredericton, N.B., Canada, 1987.

[8] F.R. Steward, D.N. Trivic, An assessment of particle radiation in a pulverized-coal-fired boiler, J. Inst. Energy 452 (1989) 138–146.

[9] M.J. Yu, S.W. Baek, J.H. Park, An extension of the weighted sum of gray gases non-gray gas radiation model to a two phase mixture of non-gray gas with particles, Int. J. Heat Mass Transfer 43 (2000) 1699–1713.

[10] T.F. Smith, Z.F. Shen, J.N. Fridman, Evaluation of coefficients for the weighted sum of gray gases model, ASME J. Heat Transfer 104 (1982) 602–608.

[11] M.F. Modest, Radiative Heat Transfer, McGraw-Hill, New York, 1993.

[12] V.P. Solovjev, B.W. Webb, An efficient method for modeling radiative transfer in multicomponent gas mixture with soot, Trans. ASME 123 (2001) 450–457.

[13] I. Ayranci, N. Selcuk, MOL solution of DOM for transient radiative transfer in 3-D scattering media, J. Quantit. Spectrosc. Radiat. Transfer 84 (2004) 409–422.

[14] P.J. Coelho, A hybrid finite volume/finite element discretization method for the solution of the radiative heat transfer equation, J. Quantit. Spectrosc Radiat. Transfer 93 (2005) 89–101.

[15] M.N. Ozisik, Radiative Transfer, A Wiley-Interscience Publication, Wiley, New York, 1973.

[16] R. Siegel, J.R. Howell, Thermal Radiation Heat Transfer, Hemisphere Publishing Corporation, New York, 1993.

[17] M.F. Modest, Radiative Heat Transfer, Academic Press, New York, 2003.

[18] J.C. Chai, Finite volume method for radiation heat transfer, Ph.D. Dissertation, University of Minnesota, Minneapolis, MN, 1994.

[19] J.C. Chai, H.S. Lee, S.V. Patankar, Finite volume method for radiation heat transfer, J. Thermophys. Heat Transfer 8 (3) (1994) 419–425.

[20] J.C. Chai, S.V. Patankar, Finite Volume Method for Radiation Heat Transfer, in: Minkowitz, Sparrow (Eds.), Advances in Numerical Heat Transfer, vol. 2, Taylor & Francis, 2000.

[21] D.N. Trivic, Modeling of 3-D non-gray gases radiation by coupling the finite volume method with weighted sum of gray gases model, Int. J. Heat Mass Transfer 47 (2004) 1367–1382.

[22] H.C. Van de Hulst, Light Scattering by Small Particles, John Wiley, Chichester, 1957.

[23] C.F. Chromey, Evaluation of Mie equations for colored spheres, J. Opt. Soc. Am. 50 (1960) 73.

[24] L. Lorenz, in: Videnscab Selscab Scrifter, vol. 6, Copenhagen, Denmark, 1890.

[25] H.C. Hottel, A.F. Sarofim, Radiative Transfer, McGrow-Hill, New York, 1967.

[26] D.N. Trivic, T.J. O'Brien, C.H. Amon, Modeling the radiation of anisotropically scattering media by coupling Mie Theory with finite volume method, Int. J. Heat Mass Transfer 47 (2004) 5765–5780.

[27] H.C. Hottel, A.F. Sarofim, Radiant heat exchange in a gas filled enclosure: allowance for non-uniformity of gas temperature, AIChE J. 4 (3) (1958).

[28] F.R. Steward, K.N. Tennankore, Towards a finite difference solution coupled with the zone method for radiative transfer for a cylindrical combustion chamber, J. Inst. Energy 52 (1979) 107–114.

[29] F.R. Steward, P. Canon, The calculation of radiative heat flux in a cylindrical furnace using Monte Carlo method, Int. J. Heat Mass Transfer 14 (1971) 245–262.

[30] F.R. Steward, H.K. Guruz, Mathematical simulation of an industrial boiler by the zone method of analysis, Proceedings of the Seminar on Heat Transfer from Flames, Scripta Publishing, Washington, DC, 1974.

[31] J.S. Kocaefe, Mathematical modeling of the interaction between flow and radiative transfer in combustion systems, M.Sc.E. Thesis, Department of Chemical Engineering, University of New Brunswick, Fredericton, N.B., Canada, 1982.

[32] D.L. Carmichael, A generalized computer model for combustion systems, M.Sc.E. Thesis, Department of Chemical Engineering, University of New Brunswick, Fredericton, N.B., Canada, 1979.

[33] K.H. Guruz, The effects of solid particles on radiant transmission in furnace enclosures, Ph.D. Thesis, Department of Chemical Engineering, University of New Brunswick, Fredericton, N.B., Canada, 1973.

[34] D. Deirmendjian, R. Clasen, V. Viezee, Mie scattering with complex index of refraction, J. Opt. Soc. Am. 51 (1961) 62.